HHS Public Access

Author manuscript

Sci Transl Med. Author manuscript; available in PMC 2019 June 29.

Published in final edited form as:

Sci Transl Med. 2017 May 03; 9(388): . doi:10.1126/scitranslmed.aad9157.

Mutations in the vesicular trafficking protein annexin A11 are associated with amyotrophic lateral sclerosis

A full list of authors and affiliations appears at the end of the article.

Abstract

Amyotrophic lateral sclerosis (ALS) is a fatal neurodegenerative disorder. We screened 751 familial ALS patient whole-exome sequences and identified six mutations including p.D40G in the *ANXA11* gene in 13 individuals. The p.D40G mutation was absent from 70,000 control whole-exome sequences. This mutation segregated with disease in two kindreds and was present in another two unrelated cases ($P = 0.0102$), and all mutation carriers shared a common founder haplotype. Annexin A11-positive protein aggregates were abundant in spinal cord motor neurons and hippocampal neuronal axons in an ALS patient carrying the p.D40G mutation. Transfected human embryonic kidney cells expressing *ANXA11* with the p.D40G mutation and other N-terminal mutations showed altered binding to calcyclin, and the p.R235Q mutant protein formed insoluble aggregates. We conclude that mutations in *ANXA11* are associated with ALS and implicate defective intracellular protein trafficking in disease pathogenesis.

INTRODUCTION

Gene hunting in rare Mendelian disorders has been transformed by exome sequencing. This approach is particularly attractive for late-onset autosomal dominant syndromes with short disease durations, such as amyotrophic lateral sclerosis (ALS), where DNA is rarely

‡ Corresponding author. chris.shaw@kcl.ac.uk.

*These authors contributed equally to this work.

†These authors contributed equally to this work.

Author contributions: B.N.S., S.D.T., C.F., H.S., H.-J.C., C.T., A.K., S.A.-S., J.E.L., M.W., V.S., and C.E.S designed the experiments. B.N.S., A.S.-G., C.V., and J.W.M. performed the exome capture. M.S. designed and implemented the exome assembly and variant calling. S.D.T. designed and implemented the variant annotation and filtering pipeline, the secondary structure analyses, and the 1000 genomes haplotype study. S.D.T. and K.P.K. managed the exome capture data. M.W. and S.D.T. designed the ExAC simulation strategy, and S.D.T. implemented it. M.L. provided the ExAC population stratification. B.N.S. performed the mutation screening, haplotype study, HEK transfection studies with ANXA11 WT and mutant constructs, cotransfection study with ANXA11 and calcyclin, protein fractionation, solubility assays, and Western blotting of lysates from postmortem tissue. C.F. cultured and transfected mouse primary motor neurons with ANXA11-HA WT and mutant constructs. H.-J.C. transfected SH-SY5Y cells and conducted the cotransfection and IP assay using ANXA11 WT and R235Q constructs. H.S. and A.S. performed the FLAG-CACY and ANXA11-GFP binding assays. C.T., A.K., W.K., D.M.D., M.N., and S.A.-S. performed the neuropathology staining and analysis. C.H.W., M.D.M., N.W.P., and P.C.S. performed the genetic screening. E.L.S. and J.C.M. conducted the data analysis. P.J.N., F.B., J.M.V.d.J., A.L.M.A.t.A., A.G.R., J.d.B., J.E.-P., C.T., F.V., S.D., N.L., H.P., K. E.M., A.A.-C., P.J.S., J.K., M.R.T., K.T., O.H., J.D.G., J.d.B., C.G., A.R., R.H.B.J., S.A.-S., N.T., V.S., J.E.L., and C.E.S. collected and/or contributed the DNA samples or exome sequences. B.N.S., S.D.T., and C.E.S. wrote the manuscript with contributions from the other authors.

Competing interests: R.H.B.J. is a consultant for Voyager Therapeutics. V.S. serves on the board of Cytokinetics for the Vitality trial in ALS and has received consulting fees. A.A.-C. has consulted for Mitsubishi Tanabe Pharma. C.E.S. is an unpaid consultant to Chronos Therapeutics. The other authors declare that they have no competing interests.

Data and materials availability: FALS exome variants generated from the cohort used in this study have been deposited for public access into the University of Massachusetts Medical School ALS Variant Server (http://als.umassmed.edu). DNA and postmortem tissue samples can be obtained by contacting the corresponding author C.E.S.

available from multiple affected individuals in the same kindred to support traditional linkage analyses. ALS has a lifetime risk of 1 in 400 and is characterized by degeneration of brain and spinal cord motor neurons resulting in progressive paralysis and death within ~3 years (1). Ten percent of ALS cases are familial (FALS), and a causative gene mutation can be identified in ~60% of European kindreds (2). Mutations in the same genes account for ~10% of sporadic ALS cases (SALS), reflecting incomplete penetrance. Nonsynonymous mutations in the *SOD1, TARDBP,* and *FUS* genes and an intronic hexanucleotide repeat expansion in *C9orf72* together account for ~20% of all ALS cases, and other rarer genes account for another ~1 to 3% of cases (3,4). Whole-genome or whole-exome sequencing (WGS/WES) has enabled identification of nine ALS genes through either shared variant segregation analysis in ALS kindreds (*VCP, PFN1, MATR3, CHCHD10,* and *CCNF)* or rare variant burden analysis *(TUBA4A, TBK1, NEK1,* and *C21orf2)* (5–15). Here, we analyzed whole-exome sequences from patients with FALS and identified a nonsynonymous founder mutation in the *ANXA11* gene that is present in all affected family members tested and is also found in multiple unrelated index cases. Annexin A11 is a widely expressed calcium-dependent phospholipid-binding protein (505 amino acids, 56 kDa) that belongs to the larger human annexin protein family of 12 members (16). Each family member has four highly conserved annexin domains, which can form complexes with calcium ions facilitating binding to anionic cell membranes. Unique to the annexin family, annexin A11 has the longest N terminus (~196 amino acids), which is hydrophobic and disordered and binds to several interacting partners, the best characterized being calcyclin (encoded by *S100A6*) (17). Annexin A11 is associated with autoimmune disorders such as systemic lupus erythematosus, and case-control studies have found a genetic association between the p.R230C single-nucleotide polymorphism (SNP) with the multisystem autoimmune disease sarcoidosis (18, 19). Additionally, increased annexin A11 expression is also found in breast cancer and other acquired malignancies (18). Here, we present a new role for annexin A11 in a rare neurodegenerative Mendelian disorder, ALS.

RESULTS

Exome sequencing detects missense *ANXA11* mutations in ALS cases

From our cohort of 751 European FALS patients (negative for *C9orf72* GGGGCC expansions), we obtained exome sequencing data for two or more affected relatives from only 50 families (average, 2.14 individuals per family), highlighting the difficulty in obtaining DNA samples from extended kindreds for this late-onset disorder. Families ranged from a simple pair of siblings (sharing an estimated 50% of their variants) to an index case, parent, and a second cousin (sharing an estimated 1.5% of their variants). On average, 84% (range, 58 to 97%) of the proteincoding bases contained in reference sequence (RefSeq) transcripts were sequenced in all family members to a depth of ≥10 reads, a cutoff threshold in line with that used by the Exome Aggregation Consortium (ExAC) for defining high-quality variants (20). Our filtering strategy was to detect new high-quality, coding and splicing variants that are absent from the 1000 genomes, UK10K, Exome Variant Server (EVS), and ExAC databases (n > 72,000). This produced an average of ~10 candidates per family (range, 0 to 27) (table S1). As proof of principle, the analysis identified mutations shared in single kindreds from several known ALS genes, including *SOD1, TARDBP, FUS,*

DCTN1, and TUBA4A (9, 21–24). It was immediately apparent that only two variants appeared in the list of candidates for more than one family: The well-characterized pathogenic p.M337V mutation in *TARDBP* (25) was found in two North American families, and a new p.D40G variant in *ANXA11* (Refseq ID NM_145869) was found in two British families (an uncle-niece pair and two cousins). (The full list of candidate variants found in both U.K. *ANXA11* p.D40G families are listed in table S2.) One additional Italian proband from the extended FALS exome cohort also carried the same *ANXA11* p.D40G variant. We then extended the analysis to include 694 unrelated European FALS probands (including the 50 probands from our multiplex families) and sought new protein-changing variants that were shared by three or more probands. This approach also identified the *ANXA11* p.D40G variant and the following well-characterized pathogenic ALS mutations: 10× *SOD1* p.I114T (26), 6× *TARDBP* p.A382T (22), 5× *SOD1* p.A5V (27), 4× *FUS* p.R521C (23), 3× *TARDBP* p.M337V, 3× *SOD1* p.G94D (28), and 3× *FUS* p.P525L (29).

We then used Sanger sequencing to sequence the coding exons of *ANXA11* in a separate set of 180 British apparent SALS cases and identified one further heterozygous p.D40G carrier, bringing the total number to 4 out of a combined cohort of 874 probands. Because the two U.K. families carrying the p.D40G mutation were not sufficiently powered to conduct a linkage analysis [simulated lod (logarithm of the odds ratio for linkage) score of 0.63 using MERLIN] (30), we sought an alternate method to ascertain the significance of the p.D40G mutation. It is possible that a variant could be present four times in a sample of 874 cases and absent from 72,000 other individuals yet still be unrelated to the disease. We therefore tested the null hypothesis that any equal-sized cohort of Europeans could also contain a new variant shared by at least four people. We achieved this by running simulation studies using the aggregated variant call counts from the non-Finnish European (NFE) subset of the ExAC database ($n = 33,370$). Briefly, all ExAC NFE variants were randomly distributed across 33,370 individuals, and random cohorts of 874 people were extracted. The cohort was deemed to have “passed” if it contained at least one protein-changing variant found four or more times within the cohort, but absent from the remainder of ExAC, UK10K, EVS, and 1000 genomes databases. After 250,000 iterations, only 2550 simulated cohorts contained such a variant, which demonstrated that the presence of the p.D40G variant was statistically significant ($P = 0.0102$). Although not population-matched to our cohort, we consider ExAC to be suitable for this purpose because it contains a high proportion of Swedes who are on average more genetically homogeneous than the U.K. population (table S3) (31). Therefore, ExAC would be expected to produce more shared nonpathogenic variants than our cohort, and so, we expect this estimate of significance to be a conservative one. In conjunction with the family-based study, the simulation analysis provides additional evidence that the *ANXA11* p.D40G mutation is associated with ALS.

The p.D40G mutation has a common European founder

Sanger sequencing of DNA from 17 family members across the two multigenerational British kindreds confirmed the presence of the p.D40G mutation in all four affected individuals identified from the exome capture data (Fig. 1, A and B). Four unaffected individuals also carried the mutation, but incomplete penetrance of ALS mutations is well recognized and three of these individuals were in their 40s, whereas the average age of

disease onset in *ANXA11* p.D40G affected carriers is 72 years of age. DNA was available from five British p.D40G carriers who share a common haplotype on the disease allele defined by four exonic SNPs and two polymorphic microsatellites spanning the locus with phase determined by a cluster of carriers in U.K. Family 2, confirming a common founder (fig. S1; primers are listed in table S4). The minimal haplotype is defined by a physical stretch of 2.5 megabases of genomic DNA spanning the *ANXA11* locus, common to all p.D40G carriers. The core four-SNP haplotype, located in exons of genes flanking *ANXA11,* is present in ~5% of our extended FALS cohort (n = 787, including *C9orf72* expansion-positive cases) and ~5% of Europeans from the 1000 genomes database (n = 514). This suggests that the mutation arose on a European background. The maximal recombination region defining the limits of the p.D40G locus is 7.1 megabases and contains 23 genes (fig. S2). Interrogation of exome sequencing data found that no p.D40G carriers shared any additional protein-changing variants in the 23 genes within this region. Of the coding bases, 70.3 to 97.2% were covered to a read depth of ≥10 for each sample, and 97.9% were covered by ≥10 reads in at least one sample (table S5). This evidence indicates that p.D40G is the sole causal exonic variant within this locus.

ANXA11 mutations in FALS and SALS cluster in the N terminus

Additional *ANXA11* variants were identified in two unrelated individuals in the FALS cohort who carried the c.112G>A, p.G38R variant (rs142083484), which was absent from local U.K. and Italian exome controls (n = 4505). Although the p.G38R variant is present in 5 of 31,804 NFE ExAC exomes, it is still significantly associated with FALS in our cohort (P = 0.004, two-tailed Fisher's exact test). New p.G175R (c.523G>A) and p.R346C (c. 1036C>T) variants were also each detected in a single index case. The p.G175R variant was shared by an affected sibling with ALS (Fig. 1C), confirming segregation with disease. All FALS cases having *ANXA11* variants were negative for exonic coding mutations in all known ALS genes including *SOD1, TARDBP, FUS, PFN1, UBQLN2, MATR3, CHCHD10, TBK1, OPTN, VAPB, ANG, SQSTM1, CCNF, TUBA4A, C21orf2, NEK1,* and *VCP.*

All coding exons of *ANXA11* underwent Sanger sequencing in an additional 180 British SALS cases (primers are listed in table S4). As previously mentioned, an additional p.D40G case was identified, as well as an individual carrying a p.G189E (c.566G>A) variant, present only once in U.K. and European controls (n = 4505) and 14 times in the ExAC NFE subpopulation (n = 33,140). p.G189E is also present once in an ALS genetic database (ALSdB; http://chgv.org/alsdb/index.jsp). The last variant, located in the first annexin domain, was a p.R235Q (c.704G>A) change absent in local controls (n = 4505) but present once as a low-quality variant call in ExAC. Notably, ALS cases carrying *ANXA11* mutations did not carry the p.R230C risk allele (rs1049550) that is associated with sarcoidosis (19). All variants found in FALS and SALS cases are listed in table S6 with control database frequencies and various computational predictions of pathogenicity.

Four of the six mutations in annexin A11 cluster with p.G38R and p.D40G within the long N terminus, implying that this region has functional importance. All mutation positions are completely conserved in mammals, and those in the annexin domains are also conserved in all currently sequenced birds, amphibians, and reptiles (Fig. 1D).

ALS cases carrying the p.D40G mutation show late disease onset and cytoplasmic immunoreactive inclusions in postmortem tissues

All patients with *ANXA11* mutations had late disease onset (average, 67 years) with a classical ALS phenotype without features of dementia (table S7). Five of six patients carrying the p.D40G variant first presented with difficulty speaking and swallowing (bulbar-onset ALS). Postmortem tissue was available from a SALS case carrying the p.D40G variant and showed classical pathological features of ALS together with a unique feature of large annexin A11-immunoreactive inclusions that were absent from other ALS cases or controls (Fig. 2). Spinal cord sections revealed marked neuronal loss within the anterior horns. There was marked myelin pallor and astrogliosis in the anterior and lateral corticospinal tracts. Many surviving motor neurons contained cytoplasmic inclusions that stained positive for p62 and phospho-TDP-43 (Fig. 2A). Phospho-TDP-43 inclusions were also found in the medulla, temporal neocortex, and hippocampus. Annexin A11 staining of spinal cord sections showed numerous neuronal cytoplasmic inclusions in the cell body and adjacent axon (Fig. 2, B to E). These included skein-like (Fig. 2B), large-caliber, tubular-shaped structures (Fig. 2, C and D), as well as filamentous and more complex basket-like inclusions (Fig. 2E). Annexin A11-positive neuronal cytoplasmic inclusions were also evident in small numbers in the motor cortex, dentate gyrus of the hippocampus, and temporal neocortex sometimes accompanied by abundant torpedo-like neuritic structures in the neuropil (Fig. 2F). Occasional sparse annexin A11-positive neuronal cytoplasmic inclusions and neurites were also seen in the occipital lobe, but no staining was observed in the cerebellum. Staining for the amyloid precursor protein, neurofilament (light, medium, and heavy), and b3-tubulin was negative. SALS cases ($n = 13$) devoid of known mutations were negative for annexin A11 neuronal cytoplasmic inclusions in the spinal cord (Fig. 2G), as were two *C9orf72* expansion-positive cases and an SOD1-positive case with a p.D101G mutation (Fig. 2, H to J). Additionally, tissue from three ALS/frontotemporal dementia (FTD) cases (Fig. 2K), three Alzheimer's disease patients (Fig. 2L), and three Parkinson's disease patients were negative for annexin A11-positive neuronal cytoplasmic inclusions in the cortex ($n = 2$) and spinal cord ($n = 1$) for ALS/FTD cases and in cortical and brainstem tissue for Alzheimer's disease and Parkinson's disease patients, respectively. Spinal cord annexin A11 staining was negative in 13 controls (Fig. 2M) (including frontal and temporal cortex and medulla regions in three controls). Double fluorescent labeling of phospho-TDP-43 and annexin A11 in spinal cord neurons showed no evidence of colocalization (Fig. 2, N and O). Some annexin A11-positive aggregates were ubiquitinated (Fig. 2P). The cytoplasmic aggregates seen in postmortem tissue from the p.D40G ALS patient may be caused by enhanced annexin A11 expression due to an additional promoter mutation. However, screening of the *ANXA11* promoter identified no new, rare or common variants [minor allele frequency (MAF), <0.05] in any of the cases carrying *ANXA11* mutations. Furthermore, in lysates prepared from frozen frontal cortex postmortem tissue from an ALS case with the p.D40G mutation, there was no change in the amount of annexin A11 compared to three age- and sex- matched controls (fig. S3).

Overexpressed mutant annexin A11 forms insoluble protein aggregates in mouse primary motor neurons

To understand the functional significance of these variants, we undertook a series of cellular studies of mutations identified in our exome set. We generated annexin $A11^{WT}$, annexin $A11^{G38R}$, annexin $A11^{D40G}$, and annexin $A11^{R235Q}$ tagged with hemagglutinin (HA) or green fluorescent protein (GFP) at the C terminus. Constructs were expressed in mouse primary motor neurons and human embryonic kidney (HEK) 293 cells. Mouse primary motor neurons transfected with annexin $A11^{WT}$ HA-tagged constructs showed nuclear and cytoplasmic localization. In the cytoplasm, annexin A11 was present in larger vesicle-like structures and smaller foci structures and was diffusely distributed throughout the soma, axons, and dendrites (Fig. 3A). Apart from annexin $A11^{R235Q}$, which was elevated in the cytoplasm, there was no evidence that the other mutations affected the distribution between the nucleus and cytoplasm (Fig. 3B) (32). Annexin $A11^{R235Q}$ mutant protein appeared to aggregate into the foci but was never associated with vesicle-like structures, and diffuse staining was absent ($P < 0.001$) (Fig. 3C). Annexin $A11^{D40G}$ had a similar pattern to wild-type (WT) protein, but annexin $A11^{G38R}$ displayed significantly less association with vesicle-like structures ($P = 0.005$). Annexin $A11^{R235Q}$ GFP-tagged protein in HEK cells showed marked aggregation into ubiquitin and p62-positive inclusions that specifically bound endogenous annexin A11 antibody, which was confirmed by Western blot (fig. S4). Annexin $A11^{R235Q}$ GFP-tagged protein also produced high-molecular weight insoluble species that were observed on Western blot (Fig. 3, D and E) ($P = 0.007$).

Annexin $A11^{R235Q}$ sequesters wild type annexin A11

We also investigated whether the aggregation-prone p.R235Q mutation recruited WT Annexin A11. Human neuroblastoma SH-SY5Y cells were cotransfected with constructs of either Annexin $A11^{WT}$ tagged with GFP and Annexin $A11^{WT}$ tagged with HA or Annexin $A11^{R235Q}$ tagged with GFP and Annexin $A11^{WT}$ tagged with HA (Fig. 4A). The merged image of cells expressing annexin $A11^{WT}$ tagged with HA and Annexin $A11^{WT}$ tagged with GFP showed nuclear staining and diffuse cytoplasmic staining (Fig. 4A, top). Annexin $A11^{R235Q}$ tagged with GFP showed cytoplasmic puncta, and the WT protein tagged with HA showed colocalization with the mutant protein (Fig. 4A, bottom). This suggests that insoluble mutant Annexin $A11^{R235Q}$ recruits WT annexin A11. This recruitment of WT annexin A11 to mutant aggregates was confirmed by conducting a solubility assay on HEK cells cotransfected with annexin $A11^{WT}$ HA tagged and either Annexin $A11^{WT}$ or Annexin $A11^{R235Q}$ tagged with GFP, followed by immunoprecipitation (IP) and Western blot analysis. For the solubility assay, only the insoluble urea fraction of the Annexin $A11^{WT}$ HA-tagged/Annexin $A11^{R235Q}$ GFP-tagged cotransfection contained Annexin $A11^{WT}$ compared to the cotransfection with Annexin $A11^{WT}$ (Fig. 4B), demonstrating that the insoluble p.R235Q mutant protein can sequester WT Annexin A11. Furthermore, we cotransfected HEK cells with HA-tagged Annexin $A11^{WT}$ and GFP-tagged Annexin $A11^{R235Q}$. We pulled down the mutant protein with rabbit anti-GFP antibody and probed the blot with mouse anti-HA antibody, which demonstrated that WT Annexin A11 coimmunoprecipitated with the insoluble mutant protein (Fig. 4C). This suggests that mutant Annexin A11 is able to recruit WT Annexin A11 and may therefore exert toxicity in a dominant-negative manner.

Annexin A11 mutant proteins do not bind to calcyclin

Residues 50 to 62 in Annexin A11 bind to calcyclin (encoded by *S100A6*) (33) and are in close proximity to the p.G38R and p.D40G mutations, so we sought evidence for any effect of the mutations on this interaction. Calcyclin is a 10-kDa protein that contains two EF-hand calcium-binding motifs (34). Secondary structure prediction analysis (using the algorithm Jpred4) (35), carried out on an alignment of all mammalian Annexin A11 ortholog sequences, predicted that residues 40 to 44 and 51 to 59 potentially form dual putative amphipathic helices, a finding that correlates with a previous investigation of recombinant mouse annexin A11 (fig. S5A) (36). The helices also mirror those seen in annexin A1, which, in the absence of calcium ions, are embedded within the annexin core but then are released upon activation by calcium ions, facilitating their binding to S100 calcium-binding protein A11 and also mediating calcium-dependent protein-membrane interactions (fig. S5, B and C) (37, 38). Although the N terminus of annexin 11 is much longer than and highly divergent from the N terminus of annexin 1, the high conservation of the first four residues in the second helix (QEYV in annexin 1 versus QDYL in annexin 11) implies a possible conserved binding site in the annexin core and is additional evidence for a similar mechanism of action. Both the Annexin A11 p.G38R and p.D40G variants are predicted to prevent or severely reduce formation of the first amphipathic helix (fig. S5D). Extending this analysis to 22 rare and common polymorphisms spanning the D40 residue and listed in ExAC, we predicted no abolition of the first or second N-terminal amphipathic helix (fig. S6), suggesting that this disruption of structure is disease-specific.

To assess the effects of mutations in annexin A11 on binding to calcyclin, we performed binding assays of GFP-tagged annexin $A11^{WT}$ and the annexin $A11^{G38R/D40G/G189E/R235Q}$ mutants using a previously published in vitro IP assay (39). Annexin $A11^{WT}$ coimmunoprecipitated with calcyclin, confirming that annexin A11 binds to calcyclin. Annexin $A11^{D40G}$ showed disruption of binding to calcyclin, as did annexin $A11^{G189E}$ and annexin $A11^{R235Q}$ mutant proteins (Fig. 5A). Annexin $A11^{G38R}$ binding to calcyclin, however, was markedly increased compared to WT annexin A11. To assess the specificity of the loss of calcyclin binding due to annexin A11 mutations, we also conducted binding assays with four *ANXA11* variants present in control individuals. These were a rare p.D40H variant (rs368751524, seen once only in ExAC) not detected in our ALS cases, two common NFE N-terminal polymorphisms flanking p.D40G—p.P8L (rs147334030; MAF, 0.007) and p.R191Q (rs2229554; MAF, 0.05)—and the p.R230C SNP associated with sarcoidosis (rs1049550;MAF, 0.44). These polymorphisms behaved in the same manner as WT annexin A11 and did not alter calcyclin binding (fig. S7). Therefore, disruption of calcyclin binding in ALS cases harboring *ANXA11* mutations is disease-specific. No differences were observed in the binding of annexin A11 to other known binding partners such as apoptosis-linked gene 2 [ALG-2 (encoded by *PDCD6*)] and sorcin (fig. S8)

Calcyclin is overexpressed in corticospinal tract astrocytes of ALS patients

Spinal cord sections from the ALS patient carrying the p.D40G mutation were stained with anti-calcyclin antibody. Although there was no observable difference in neuronal staining between the ALS case and controls, increased calcyclin expression was detected in the cytoplasm of astrocytes in the lateral corticospinal tracts compared to controls (Fig. 5B, i

and ii). This was not a mutation-specific event because elevated calcyclin expression was also seen in apparent SALS cases without known ALS mutations (Fig. 5B, iii). Increased expression of calcyclin in astrocytes of the corticospinal tract has previously been reported in SALS cases, as well as in $SOD1^{G93A}$ transgenic mice, but the functional significance of this observation is unknown (40, 41).

Overexpression of calcyclin prevents aggregation of p.R235Q mutant annexin A11

We also explored the impact of calcyclin interactions on annexin A11 solubility. We cotransfected FLAG-tagged $calcyclin^{WT}$ with GFP-tagged annexin $A11^{WT}$ or annexin $A11^{R235Q}$ in HEK cells and assessed annexin A11 solubility using the NP-40 insolubility assay and Western blot analysis. Remarkably, the increase in calcyclin expression reduced soluble WT and p.R235Q annexin A11 but cleared insoluble annexin $A11^{M35Q}$ (Fig. 5C). This suggested that increasing calcyclin may inhibit annexin A11 expression or enhance annexin A11 clearance through a degradation pathway. Treating the cotransfected cells with the ubiquitin proteasome inhibitor MG132 for 24 hours restored annexin $A11^{M35Q}$ insolubility (Fig. 5D; $P < 0.001$).

DISCUSSION

Using a stringent filtering strategy on a large cohort of FALS exome sequences ($n = 694$) in conjunction with a shared variant analysis of 50 Caucasian kindreds, we identified a nonsynonymous mutation p.D40G in *ANXA11,* shared in two U.K. families but absent from >70,000 control exome sequences. The mutation segregated with disease within the families and was detected in an additional Italian FALS proband. Sequencing of 180 unrelated U.K. SALS patients identified p.D40G in a sixth individual, providing further evidence that p.D40G is associated with ALS.

Our study was limited by two factors. First, the primary shared variant analysis that formed the basis of the study relied on the pathogenic variant for each family being a nonsense, missense, or splicing mutation located in a region sequenced to an adequate depth in all family members. Second, because we lacked power to perform traditional linkage within our p.D40G kindreds, we devised a simulation-based approach to model the number of new variants that would be found by chance multiple times in a disease cohort of this size. Using this strategy, we were able to demonstrate that the p.D40G mutation is associated with ALS in the four kindreds ($P = 0.0102$). In addition, all p.D40G individuals had a common founder p.D40G haplotype, which adds to the growing list of founder ALS mutations (42–44). A new p.G175R mutation segregated with disease in another kindred; several different *ANXA11* mutations clustered in the N terminus of the molecule were also associated with ALS, which implicates a functional impact of mutations in this region.

Mutations in *ANXA11* present a clinical phenotype characterized by late-onset classical ALS with five of six p.D40G cases having bulbar-onset disease. Postmortem tissue from a p.D40G ALS case displayed abundant annexin A11-positive aggregates within motor neurons in the spinal cord and in neurons and neuropil in the neocortex and hippocampus in addition to the classical features of neuronal loss, phospho-TDP-43 inclusions, and astrogliosis.

Annexin A11 is a phospholipid-binding protein that forms phospholipid vesicles in vitro in a calcium-dependent manner (36). It may participate in vesicle trafficking, but it has also been reported to play a role in apoptosis, exocytosis, and cytokinesis (18, 36). Annexin A11 colocalizes with calcyclin in the nuclear envelope during prophase of mitosis (45); however, little is known about its role in postmitotic neurons.

Our cellular expression studies indicate that annexin A11 does form vesicle-like structures in motor neurons, providing circumstantial evidence for a role in vesicular transport (Fig. 3). Annexin A11 has recently been shown to participate in regulating the delivery of vesicular cargoes from the endoplasmic reticulum to the Golgi apparatus, which is mediated through annexin A11 binding to ALG-2 to stabilize Sec31A (46). In our study, however, annexin A11 mutations did not directly affect binding to ALG-2 in IP assays.

Annexin A11 mutations could behave in a dominant-negative manner and interfere with the normal function of WT annexin A11. We have demonstrated the sequestration of WT annexin A11 into aggregates with the p.R235Q mutant annexin A11. We also observed a large number of annexin A11 inclusions in affected neurons in postmortem tissue from a patient carrying the p.D40G mutation, which is consistent with a dominant-negative mechanism. Most *ANXA11* mutations are, however, in the N terminus and do not appear to alter solubility or induce aggregation in cultured cells. The p.D40G and p.G38R mutations lie close to the calcyclin-binding domain in annexin 11. Calcyclin is known to play a role in proteostasis, during which it forms a functional complex with calcyclin-binding protein (CACYBP) and the RING-type E3 ubiquitin ligase SIAH-1 that regulates ubiquitination and degradation of many proteins including β-catenin (47). We observed significant differences in calcyclin binding with several annexin A11 mutations. Calcyclin binding was inhibited by p.D40G and p.G189E mutations but was consistently increased above that for WT by the p.G38R mutation. Therefore, loss of calcyclin binding may result in an accumulation of cytoplasmic annexin A11, promoting formation of insoluble aggregates. Because most N-terminal mutations abolished calcyclin binding, this suggested that calcyclin may also be necessary for annexin A11 structure and function and that N-terminal mutations may therefore act through a loss-of-function mechanism. Although the p.R235Q mutant annexin A11 also failed to bind to calcyclin (possibly because of aggregation), it is interesting to note that the overexpression of calcyclin led to clearance of insoluble p.R235Q annexin A11 aggregates by facilitating proteasomal degradation. Because p.R235Q mutant annexin A11 is able to sequester WT annexin A11, it could also disrupt binding of the WT protein to calcyclin in the same manner as the p.D40G mutation; therefore, a dominant-negative loss of function could be a common mechanism.

We and others have shown that calcyclin expression is increased in astrocytes in apparent SALS cases, as well as in the patient carrying the p.D40G mutation (40, 41). Although this phenomenon is not solely linked to *ANXA11* mutations, it raises the possibility that increased astrocytic calcyclin expression is a response to defective proteostasis. Cells in which TDP-43 is knocked down demonstrate increased expression of calcyclin transcripts (48, 49). Additionally, elevated calcyclin concentrations can lead to formation of oligomers that have amyloidogenic properties that may seed superoxide dismutase 1 (SOD1) aggregation (50).

In summary, we have identified six rare *ANXA11* variants in 13 individuals, which account for ~1% of familial and 1.7% of apparent SALS cases in our cohort. Functional investigation of four of these variants (p.G38R, p.D40G, p.G189E, and p.R235Q) yielded initial insights into a causative role in ALS biology. However, the contribution of the remaining *ANXA11* variants to disease has yet to be determined. *ANXA11* variants altered binding to calcyclin, which led to aggregation of annexin A11 in the cytoplasm of transfected cells and in neuronal cytoplasmic inclusions in postmortem spinal cord and brain tissue from ALS patients. The identification of *ANXA11* variants further implicates calcium-binding proteins and intracellular trafficking in ALS pathobiology (51). Further work investigating how annexin A11 mutations affect the folding of annexin A11, its binding to calcyclin, vesicular transport, and TDP-43 aggregation will help to clarify the underlying mechanisms of disease pathogenesis.

MATERIALS AND METHODS

Study design

The aims of this study were to (i) identify genes harboring dominant Mendelian mutations that cause FALS and (2) assess the impact of those mutations in functional cellular assays and in postmortem tissues. Sample size was based on availability of DNA from fully consented FALS cases in which known pathogenic mutations had been excluded. Through international collaborations, we analyzed the exome sequences of 694 probands, which is the largest single data set from FALS cases with European ancestry. The exome data were filtered to exclude likely false-positive variant calls, any variants observed in databases of non-ALS individuals, and variants observed only in patients of a single nationality. Two parallel approaches were taken to find associated genes: (i) variants that segregated in all affected relatives within a family and were also found in more than 1 of the 50 families to which these criteria could be applied, and (ii) variants that were found in three or more unrelated probands. A set of 180 SALS cases was used as a replication cohort and screened for the presence of any variants identified in the discovery phase. The significance of the association between any identified variants and ALS was estimated by simulating large numbers of random cohorts of 874 European individuals extracted from the ExAC database of variant frequencies and observing the proportion of these cohorts that supported the null hypothesis, that is, the proportion that contained a variant private to the simulated cohort and present in an equal or greater number of individuals than the associated variant.

The results implicated a missense variant, p.D40G, which was located close to a calcyclin-binding site in the protein encoded by the gene *ANXA11.* As per the second aim of the study, we then functionally characterized the effects of this mutation and other private *ANXA11* variants to explore putative disease mechanisms. This included overexpression studies in HEK and SH-SY5Y cells, in vitro binding assays with calcyclin, the major known binding partner of ANXA11, IP assays, staining of spinal cord postmortem tissue for ANXA11 inclusions and calcyclin expression, in vitro aggregation assays, and predicted alterations to the secondary structure of the ANXA11 protein.

DNA samples

Full patient consent was provided by FALS and SALS index patients and control individuals for research purposes. All patients had a diagnosis of definite or probable ALS based on revised El Escorial criteria (52) with at least one relative known to have ALS and/or FTD. All FALS patients were prescreened for the *C9orf72* intronic hexanucleotide expansion, and any positive samples were excluded from this analysis. The discovery cohort was composed of 694 FALS probands sourced from the United States (266), U.K. (193), Italy (138), Spain (33), Germany (25), Ireland (17), Canada (9), Netherlands (9), Belgium (3), and New Zealand (1). An additional 60 affected relatives of these probands, representing 50 families, also underwent exome sequencing in tandem for segregation analysis. Sequence data for 102 of the cases in the cohort were obtained, with permission, from the dbGAP (database of Genotypes and Phenotypes) repository [National Institutes of Health (NIH) Exome Sequencing of FALS, National Institute of Neurological Disorders and Stroke (NINDS), phs000101. v4.p1, Traynor].

Exome sequencing and bioinformatic analysis

Paired-end FASTQ files from Illumina exome sequencing were aligned to the hg19 human reference using Novocraft NovoAlign and variants called with SAMtools v1.1 mpileup. VCF files were filtered at DP ≥ 10, GQ ≥ 20, and MQ ≥ 50, and indels were normalized with bcftools v1.1 norm. Functional annotation, pathogenicity predictions, and matches to 1000 genomes were added with table_annovar.pl (53), whereas all other annotation was added via custom perl scripts. Variants were filtered out if they were not novel [defined as being present in either 1000 genomes (www.1000genomes.org), ExAC (http://exac.broadinstitute.org/), Exome Sequencing Project (http://evs.gs.washington.edu/EVS/), UK10K (www.uk10k.org/), or 672 in-house exome controls] or if they were located at positions with a read depth <10 in >25% of ExAC samples. Insertions and deletions were excluded because of the increased error rate in matching variants to control databases assembled and called by alternative pipelines. Synonymous and intronic variants were assessed by NetGene2 and GeneSplicer and excluded if no changes in scores compared to the reference allele were observed at locations matching to known Refseq acceptor or donor splice sites. Common ancestry between samples was taken from existing familial annotation where available and also deduced from IBD analysis in PLINK v1.07 (54). Two parallel approaches were then taken to narrow down this set of high-quality, novel, protein-changing variants to those most likely to be pathogenic in ALS. First, we identified the variants that were shared between all exome-sequenced cases of the 50 families for which data were available for more than one family member, an approach used successfully in many Mendelian disorders (55). Second, we identified all the variants that were shared by three or more probands, selected as the sample from each of the 694 families with the highest proportion of the exome covered at a depth ≥10×. The read alignments were manually inspected for all resulting variants, and clearly identifiable false positives were removed, resulting in an effective revised filter cutoff of GQ ≥90.

Simulation studies using ExAC variant calls

To assess the null hypothesis, that finding a novel protein-changing variant four or more times would also likely to occur in a nondisease cohort, we chose a simulation strategy on the basis of variant calls from the ExAC database. The VCF files for the r.0.3 release of ExAC were annotated and filtered by the identical pipelines described above, with the exception that only variants present within the NFE population of ExAC samples were considered. ExAC NFE heterozygote and homozygote counts were added together to give NFE carrier counts. The data were then further filtered to only retain variants shared by four or more carriers (n = 67,154). These variants were then randomly distributed across 33,370 simulated ExAC European individuals. The FALS + SALS cohort was then simulated by randomly selecting 874 of these individuals (694 FALS probands +180 SALS) from the total pool. To replicate the variant that is novel across the remainder of the data set, each variant in the filtered ExAC data set was rejected if all NFE carriers were not within the simulated cohort. A cohort was deemed to have passed if at least one variant met the above criteria. The P value was calculated as the proportion of cohorts that passed, after sufficient permutations of random cohorts had been generated to achieve a stable result to two significant figures. All random integers were generated using the perl CPAN Math::Random::Secure irand function.

Genetics screening

All coding exons of *ANXA11* (Refseq ID NM_145869) were amplified using standard polymerase chain reaction (PCR) procedures. At least 100 base pairs of flanking intronic sequence was included to detect splice site mutations (primers are listed in table S4). Amplicons were directly sequenced with BigDye Terminator v1.1 on an ABI 3130 genetic analyzer (Applied Biosystems Pty Ltd.), and sequence chromatograms were analyzed for mutations using Sequencher 4.10 directly by eye (Gene Codes Corporation). Reconfirmation of novel mutations was conducted by redilution of stock DNA and re-PCR and direct sequencing. Rare variant positions in *ANXA11* were also filtered against 3596 Italian exome controls. A total of 909 local control U.K. samples matched for sex and age were assayed for *ANXA11* genomic SNP positions for the p.G38R, p.D40G, p.G189E, and p.R235Q mutations using KASPar genotyping methods by LGC Genomics.

Haplotype study

Microsatellites surrounding the ANXA11 locus were identified using Hg19 build of the University of California, Santa Cruz Genome Browser (www.genome.ucsc.edu/) and amplified by standard PCR with the forward primer incorporating a fluorescent 6-carboxyfuorescein (FAM) label. One microliter of PCR product was run using fragment analysis on an ABI 3130 genetic analyzer. Allele sizing was conducted using GeneMapper V4. SNP markers rs41291392, rs17617713, rs72821609, and rs72805713 were genotyped using standard PCR and direct sequencing (primers are listed in table S4). The genomic haplotype locus figure (fig. S2) was drawn using the “Dalliance” program (56).

Plasmids and cloning

A complementary DNA (cDNA) encoding ANXA11 was amplified from pEGFP-C3/ANXA11 (57) with the following pair of oligonucleotides with a *Bam* HI site (underlined): 5′-TAGGATCCACCATGAGCTACCCTGGCTATCC-3′ (sense) and 5′-GCGGATCCGAGTCATTGCCACCACAGATCTT-3′ (antisense). The DNA fragment obtained was subcloned into the pCR-Blunt II-TOPO (Invitrogen). To construct pANXA11-GFP, a *Bam* HI fragment from pCR-Blunt II-TOPO/ANXA11 was inserted into the *Bam* HI site of pEGFP-N-SGG (58). Single-amino acid changes (G38R, D40G, and R235Q) were introduced into pANXA11-GFP by PCR-based site-directed mutagenesis. To construct pFLAG-S100A6, we inserted an *Eco* RI fragment of pCR2.1 TOPO/S100A6 (provided by K. Hitomi, Nagoya University, Japan) into the *Eco* RI site of pCMV3xFLAG-B (59). A cDNA encoding sorcin was amplified from human fetus cDNA library (Clontech) and subcloned into the pCMV-Tag 2A (Stratagene) to construct pFLAG-sorcin. An expression vector encoding ALG-2 N-terminally tagged with FLAG (pFLAG-ALG-2 RNAi^{R}) was described previously (60).

ANXA11 expression vectors (Gateway pcDNA3.1/nV5-DEST, Invitrogen) encoding C-terminal HA-tagged ANXA1 WT, p.G38R, p.D40G, and p.R235Q mutants were used in this study. Site-directed mutagenesis was performed according to the manufacturer's protocol (QuikChange II Site-Directed Mutagenesis Kit, Stratagene) using an ANXA11-HA-tagged pDONR221 entry clone plasmid to produce constructs harboring the novel mutants identified in this study. The pDONR221-ANXA11 mutant constructs were then recombined with pT-REx-DEST30 to create the final mutant expression constructs. All constructs were verified by sequencing.

Antibodies

Mouse monoclonal anti-GFP at ½000 (cat. no sc-9996, Santa Cruz Biotechnology), mouse monoclonal anti-glyceraldehyde-3-phosphate dehydrogenase (GAPDH) (cat. no G8795, Gillingham), and mouse monoclonal histone H3 (cat. no 96C10, New England Biolabs) were used for detecting lysate, soluble, and insoluble fractions on Western blot from NP-40 insolubility assays. In the annexin A11/EF-hand protein (calcyclin, ALG-2, and sorcin) binding assays, mouse monoclonal anti-FLAG (cat. no. F3165, Sigma-Aldrich) was used to immunoprecipitate FLAG-tagged EF-hand proteins, and mouse monoclonal anti-GFP (cat. no. sc-9996, Santa Cruz Biotechnology) and mouse monoclonal anti-FLAG or rabbit polyclonal anti-FLAG (cat. no. F7425, Sigma-Aldrich) were used to detect GFP-fused proteins and FLAG-tagged proteins, respectively. Polyclonal rabbit anti-ANXA11 (cat. no. 10479–2-AP, Proteintech) was used for ANXA11^{R235Q} staining of HEK cells (fig. S4) and spinal cord of the p.D40G SALS patient, SALS patient devoid of known ALS causing mutation, other neurodegenerative disorders, and controls. Polyclonal rabbit anticalcyclin (cat. no. 10245–1-AP, Proteintech) was used for immunohistochemistry (IHC) of patient and control postmortem tissue and detection of FLAG-tagged calcyclin by Western blot in HEK cells.

Transfection of HEK and SH-SY5Y cells

HEK293T and SH-SY5Y cells were maintained in Dulbecco's modified Eagle's medium (DMEM) with high glucose plus GlutaMAX and DMEM/F-12, respectively (Life Technologies), with 10% fetal bovine serum, penicillin (100 U/ml), and streptomycin (100 mg/ml) in a water-jacketed incubator at 5% CO_2. For solubility fractionation, transfections were performed in 12-well plates with 500 ng of plasmid DNA and 1.5 ml of FuGENE HD (Promega) per well according to the manufacturer's protocol. For immunofluorescence, HEK293T cells were plated at 25,000 cells/cm^2 on 13-mm-diameter, 1.5-mm-thick coverslips coated with poly-D-lysine (Sigma-Aldrich) in 24-well plates and transfected with 250 ng of DNA and 0.75 ml of FuGENE HD. SH-SY5Y cells were transfected in the same manner except that the transfection reagent used was Lipofectamine (Fisher Scientific).

FLAG-S100A6 and ANXA11-GFP binding assays

HEK293 YS14 cells (a subcloned HEK293 cell line) (61), which had been plated on the previous day, at a density of 1.8×10^6 cells per 10-cm dish were transfected with expression plasmids using polyethyleneimine (150 μg) (Polysciences) and then cultured for 24 hours. To attain equivalent expression level, we used the following amounts of plasmid DNA for SGFP2-fused proteins: 3 μg of pSGFP2-N-SGG, 5 μg of pANXA11^{WT}-SGFP2, 6 μg of p.G38R, 7 μg of p.D40G, 6 μg of p.G189E, 10 μg of p.R235Q, 5 μg of p.P8L, 5 μg of p.D40H, 5 μg of p.R191Q, and 5 μg of p.R230C. The cells were washed and harvested with phosphate-buffered saline (PBS), suspended in 210 μl per 10-cm dish (for cells expressing SGFP2-fused proteins in the case of interaction with calcyclin), 470 μl per 10-cm dish (for cells expressing SGFP2-fused proteins in the case of interactions with ALG-2 or sorcin), or in 350 μl per 10-cm dish (for cells expressing FLAG-tagged proteins) of lysis buffer [20 mM Hepes-KOH (pH 7.2), 142.5 mM KCl, and 2.5 mM $MgCl_2$] containing 0.2% Triton X-100, 10 μM EGTA, protease inhibitors [1 μM E64, leupeptin (3 μg/ml), 0.1 mM Pefabloc, 2 μM pepstatin A, and 0.2 mM phenylmethylsulfonyl fluoride], and phosphatase inhibitors (50 mM NaF, 10 mM β-glycerophosphate, and 1 mM Na_3VO_4). After 30 min on ice, the cell lysates were centrifuged at 15,000*g* for 10 min at 4°C. The cleared lysates of the cell expressing GFP-fused proteins were divided into aliquots of 200 μl and mixed with 100 μl of the cleared lysates of the cells expressing FLAG-tagged proteins. Twenty microliters of the mixture was taken as input. The samples were rotated at 4°C for 90 min in the presence of 100 μM $CaCl_2$, mixed with 0.8 μg of mouse antibody against FLAG (M2) (cat. no F7425, Sigma-Aldrich), and rotated at 4°C for further 60 min. Then, the samples were incubated overnight at 4°C with 10 μl of Dynabeads Protein G (Novex and Invitrogen). The beads were collected using a magnet and washed twice with 500 μl of lysis buffer containing 0.1% Triton X-100 and 100 μM $CaCl_2$. Washed beads were boiled for 5 min in 56 μl of 1× SDS-polyacrylamide gel electrophoresis sample buffer. Four microliters of input and 8 μl of IP (for detection of FLAG-tagged proteins) or 1.2 μl of input and 12 μl of IP (for detection of GFP-fused proteins) were run on a Western blot.

FLAG-calcyclin and ANXA11-GFP overexpression in HEK cells

Five hundred nanograms of ANXA11-GFP^{WT} and ANXA11-GFP^{R235Q} constructs was cotransfected with 500 ng of FLAG-calcyclin in a six-well dish of HEK cells plated at

25,000 cells/cm^2. Untreated ANXA11-GFP^{WT} and ANXA11-GFP^{R235Q} were cotransfected with an empty pEGFP-C1 vector (Clontech Pty Ltd.). Duplicate wells of ANXA11-GFP^{WT} and ANXA11-GFP^{R235Q} transfected cells were also treated with 0.5 μM MG132 24 hours before harvesting (48 hours after transfection). Cells were harvested and processed according to the NP-40 insolubility assay below.

Culture of mouse primary motor neurons

Motor neurons were isolated from mouse embryos, cultured, and transfected as described (62). Cells were fixed 1 or 4 days after transfection and processed for immunofluorescence. After antigen retrieval in citrate buffer for 20 min and blocking in 5% bovine serum albumin (BSA) for 1 hour, cells were hybridized overnight at 4°C with HA primary antibody (Covance, 1:1000) and were incubated with Alexa 488- or Alexa 594-conjugated secondary antibodies (Jackson Immunoresearch) for 1 hour at room temperature. Vesicles were defined as structures with a diameter between 0.5 and 1.9 μm (mean, 1 μm) and foci between 0.16 and 0.5 μm (mean, 0.3 μm).

Protein fractionation, insolubility assay, and Western blot

ANXA11-GFP WT and mutant construct-transfected HEK cells were harvested at 48 wells after transfection and fractionated using an NP-40 solubility assay as described previously (63). Lysate and soluble fractions were quantified using a BSA standard protein assay and 5 μg of lysate and soluble fractions analyzed by Western blotting. The same volume of insoluble fraction was loaded as per cell lysate. Nitrocellulose membranes were probed with mouse monoclonal anti-GFP at 1:2000 dilution, mouse monoclonal anti-GAPDH at 1:2000 dilution, and mouse monoclonal histone H3 at 1:1000 dilution in 1% skim milk and PBS-Tween. Band intensities were quantified using ImageJ (http://imagej.nih.gov/ij/). Membrane imaging was conducted with fluorescent secondary antibodies, goat anti-rabbit, and anti-mouse IgG (H + L) DyLight 680 Conjugate (cat. nos. 35568 and 35521, Thermo Life Sciences) on a LI-COR Odyssey Imager. Fifteen micrograms of frontal cortex lysate was run on polyvinylidene difluoride membranes, probed with ¼00 Proteintech rabbit ANXA11, developed using enhanced chemiluminesence, and visualized using anti-rabbit chemiluminescent horseradish peroxidase (cat. no. WBKLS0500, Millipore Immobilon).

Cotransfection IP assay

Individual wells of a six-well plate were seeded with HEK cells and transfected at 70% confluence with either annexin A11-GFP^{R235Q} or annexin A11-GFP^{R235Q} plasmid. A duplicate set of wells with annexin A11-$_{GFP}$^{WT} or annexin A11-GFP^{R235Q} were cotransfected with annexin A11-HA^{WT}. At 48 hours, cells were harvested in immunopurification buffer [50 mM tris (pH 7.4), 150 mM NaCl, 1% Triton X-100, and 100 μM $CaCl_2$ with protease and phosphatase inhibitors]. The cell lysate was collected and incubated with an immunopurification antibody (rabbit anti-GFP, cat. no AB290, Abcam) and Dynabeads Protein G (Life Technologies) overnight at 4°C. The Dynabeads Protein G antibody-protein complex was purified using magnetic separation and washed with immunopurification buffer before elution in loading buffer [variation on protocol described in (64)]. Lysates, IP, and flow-through fractions were run on a nitrocellulose membrane, and

membrane imaging was conducted with fluorescent secondary antibodies and a LI-COR Odyssey.

Mutation modeling and Jpred analysis

The Refseq protein database was searched with human ANXA11 (NP_001148.1) via BlastP at the National Center for Biotechnology Information (http://blast.ncbi.nlm.nih.gov/Blast.cgi). The highest matching sequence per vertebrate species from the first 250 results was aligned with all others using Muscle (www.ebi.ac.uk/Tools/msa/muscle/). Sequences were removed if they had a better reciprocal match to a different human annexin gene or if they contained significant numbers of gaps, mismatching regions, or consecutive "X"s, implying incomplete or mistranslated sequence. Fish were also excluded because they consistently showed significant divergence along the majority of the N terminus, and with the exception of the first 20 amino acids, a satisfactory alignment to other taxonomic classes could not be obtained. The resulting multiple alignment was hand-edited in GeneDoc and submitted to Jpred4 (www.compbio.dundee.ac.uk/jpred4/) for secondary structure prediction. Predictions were also made for the ALS-associated variants p.G38R and p.D40G and 22 non-ALS variants from the ExAC database flanking these residues, by replacing every amino acid in the multiple alignments with the variant residue. Possible amphipathicity of any resulting α helices was tested by submitting the sequences to Helixator (www.tcdb.org/progs/helical_wheel.php). The procedure was then repeated for human *ANXA1,* but with this gene, it was not necessary to exclude fish species from the alignment.

Neuropathology

Brain tissue samples in 10% formalin-fixed, paraffin-embedded tissue blocks were available from the London Neurodegenerative Diseases Brain Bank (King's College London, U.K.). Consent for autopsy, neuropathological assessment, and research was obtained from all subjects, and all studies were carried out under the ethical approval of the tissue bank. Block taking for histological and immunohistochemical studies and neuropathological assessment for neurodegenerative diseases was performed in accordance with standard criteria.

Immunohistochemistry—IHC was carried out in accordance with previously published protocols (65). Briefly, sections of 7-μm thickness were cut from the paraffin-embedded tissue blocks and deparaffinized in xylene, endogenous peroxidase was blocked by 2.5% H_2O_2 in methanol, and IHC was performed. To enhance antigen retrieval, sections were kept in citrate buffer for 10 min after microwave treatment. After blocking in normal serum, primary antibody was applied overnight at 4°C.

After washes, sections were incubated with biotinylated secondary antibody (DAKO), followed by avidin/biotinylated enzyme complex (Vectastain Elite ABC kit, Vector Laboratories). Finally, sections were incubated for 10 to 15 min with 3,3′-diaminobenzidine chromogen (0.5 mg/ml) (Sigma-Aldrich Company Ltd.) in tris-buffered saline (pH 7.6) containing 0.05% H_2O_2. Sections were counterstained with Harris's hematoxylin, and immunostaining was analyzed using a Leica microscope (Leica).

Double immunofluorescence—Seven-micrometer sections were cut from formalin-fixed paraffin-embedded blocks, dewaxed in xylene, and dehydrated in 99% industrial methylated spirit. Sections were then pretreated by microwaving in citrate buffer and blocked using normal goat serum (1:10 for 45 min). Primary antibodies were then applied, and sections were incubated at 4°C overnight. Sections were washed, and secondary Alexa Fluor antibody (Invitrogen) was applied for 45 min (in dark). Autofluorescence was quenched by incubating the sections with Sudan Black for 10 min, followed by numerous washes in PBS before coverslip mounting using hard-set media with DAPI (4′,6-diamidino-2-phenylindole). Sections were visualized using a fluorescence microscope (Zeiss Axiovert S100), and images were captured using Image-Pro Express (V6).

Statistical analysis

Statistical analysis of mouse primary motor neuron immunofluorescence data, NP-40 insolubility data, and fluorescence-activated cell sorting survival data was performed with GraphPad Prism software. Normality of the data sets was assessed with the D'Agostino-Pearson test. One-way ANOVA with Dunnett's post hoc test or Kruskal-Wallis with Dunn's post hoc test was performed depending on normality.

Supplementary Material

Refer to Web version on PubMed Central for supplementary material.

Authors

Bradley N. Smith[1,*], Simon D. Topp[1,*], Claudia Fallini[2,*], Hideki Shibata[3,*], Han-Jou Chen[1,*], Claire Troakes[1], Andrew King[1], Nicola Ticozzi[4,5], Kevin P. Kenna[2], Athina Soragia-Gkazi[1], Jack W. Miller[1], Akane Sato[3], Diana Marques Dias[1], Maryangel Jeon[2], Caroline Vance[1], Chun Hao Wong[1], Martina de Majo[1], Wejdan Kattuah[1], Jacqueline C. Mitchell[1], Emma L. Scotter[6], Nicholas W. Parkin[7], Peter C. Sapp[2], Matthew Nolan[1], Peter J. Nestor[8], Michael Simpson[9], Michael Weale[9], Monkel Lek[10,11], Frank Baas[12], J. M. Vianney de Jong[12], Anneloor L. M. A. ten Asbroek[12], Alberto Garcia Redondo[13], Jesús Esteban-Pérez[13], Cinzia Tiloca[4,5], Federico Verde[4,5], Stefano Duga[14,15], Nigel Leigh[16], Hardev Pall[17], Karen E. Morrison[18], Ammar Al-Chalabi[1], Pamela J. Shaw[19], Janine Kirby[19], Martin R. Turner[20], Kevin Talbot[20], Orla Hardiman[21], Jonathan D. Glass[22], Jacqueline de Belleroche[23], Masatoshi Maki[3], Stephen E. Moss[24], Christopher Miller[1], Cinzia Gellera[25], Antonia Ratti[4,5], Safa Al-Sarraj[1], Robert H. Brown Jr.[2], Vincenzo Silani[4,5,†], John E. Landers[2,†], and Christopher E. Shaw[1,†,‡]

Affiliations

[1]United Kingdom Dementia Research Institute Centre, Maurice Wohl Clinical Neuroscience Institute, Institute of Psychiatry, Psychology and Neuroscience, King's College London, 125 Coldharbour Lane, Camberwell, SE5 9NU London, U.K. [2]Department of Neurology, University of Massachusetts Medical School, Worcester, MA 01605, USA. [3]Department of Applied Molecular Biosciences, Graduate School of Bioagricultural Sciences, Nagoya University, Furo-cho, Chikusa-ku, Nagoya

464-8601, Japan. [4]Department of Neurology and Laboratory of Neuroscience, Istituto di Ricovero e Cura a Carattere Scientifico (IRCCS) Istituto Auxologico Italiano, 20149 Milan, Italy. [5]Department of Pathophysiology and Transplantation, “Dino Ferrari” Center, University of Milan, 20122 Milan, Italy. [6]Centre for Brain Research, Faculty of Medical and Health Sciences, University of Auckland, 85 Park Road, Grafton, Auckland, New Zealand. [7]Molecular Genetics Laboratory, Viapath, Genetics Centre, Guy’s Hospital, Great Maze Pond, SE1 9RT London, U.K. [8]German Center for Neurodegenerative Diseases, Leipziger Str. 44, 39120 Magdeburg, Germany. [9]Medical & Molecular Genetics, Division of Genetics and Molecular Medicine, King’s College London, Guy’s Tower, London Bridge, SE1 9RT London, U.K. [10]Analytic and Translational Genetics Unit, Massachusetts General Hospital, Boston, MA 02114, USA. [11]Program in Medical and Population Genetics, Broad Institute of Massachusetts Institute of Technology and Harvard, Cambridge, MA 02142, USA. [12]Department of Genome Analysis, University of Amsterdam, Academic Medical Centre, P.O. Box 22700, 1100DE Amsterdam, Netherlands. [13]Unidad de ELA, Instituto de Investigación Hospital 12 de Octubre de Madrid, SERMAS, and Centro de Investigación Biomédica en Red de Enfermedades Raras (CIBERER), U-723 Madrid, Spain. [14]Department of Biomedical Sciences, Humanitas University, Rozzano, Milan, Italy. [15]Humanitas Clinical and Research Center, Via Manzoni 56, 20089 Rozzano, Milan, Italy. [16]Trafford Centre for Medical Research, Brighton and Sussex Medical School, BN1 9RY Brighton, U.K. [17]School of Clinical and Experimental Medicine, College of Medical and Dental Sciences, University of Birmingham, Birmingham, U.K. [18]University of Southampton, Southampton General Hospital, SO16 6YD, UK. [19]Sheffield Institute for Translational Neuroscience, University of Sheffield, Sheffield, U.K. [20]Nuffield Department of Clinical Neurosciences, John Radcliffe Hospital, Oxford, U.K. [21]Academic Unit of Neurology, Trinity Biomedical Sciences Institute, Trinity College Dublin, Dublin, Republic of Ireland. [22]Department of Neurology, Center for Neurodegenerative Disease, Emory University School of Medicine, Atlanta, GA 30322, USA. [23]Neurogenetics Group, Division of Brain Sciences, Imperial College London, Hammersmith Hospital Campus, Burlington Danes Building, Du Cane Road, W12 0NN London, U.K. [24]Institute of Ophthalmology, University College London, 11-43 Bath Street, EC1V 9EL London, U.K. [25]Unit of Genetics of Neurodegenerative and Metabolic Diseases, Fondazione IRCCS Istituto Neurologico “Carlo Besta,” 20133 Milan, Italy.

Acknowledgments

We would like to thank people with ALS and their families for their participation in this project. We acknowledge sample management undertaken by Biobanking Solutions funded by the Medical Research Council at the Centre for Integrated Genomic Medical Research, University of Manchester. Postmortem tissues were provided by Medical Research Council London Neurodegenerative Diseases Brain Bank. **Funding:** Funding for this work was provided by the Middlemass family, Heaton-Ellis Trust, Motor Neurone Disease Association, Medical Research Council, The Psychiatry Research Trust of the Institute of Psychiatry, Guy’s and St. Thomas’ Charity, the Wellcome Trust, and the Noreen Murray Foundation. This work was supported by the UK Dementia Research Institute which is funded by the Medical Research Council, Alzheimer’s Society and Alzheimer’s Research UK. This is a European Union Joint Programme Neurodegenerative Disease Research (JPND) project. The project is supported through the

following funding organizations under the aegis of JPND (www.jpnd.eu): U.K. Medical Research Council and Economic and Social Research Council. This project is funded by the Medical Research Foundation (MRF) with salary provided for B.N.S. (MRF-060–0003-RG-SMITH). C.E.S. and A.A.-C. received salary support from the National Institute for Health Research (NIHR) Dementia Biomedical Research Unit at South London and Maudsley National Health Service (NHS) Foundation Trust and King's College London. C.F. received salary support from the ALS Association (ALSA). H.S. and M.M. were supported by the Japan Society for the Promotion of Science grants (15K07384 to H.S. and 26292050 to M.M.). P.C.S. was supported through the auspices of H. Robert Horvitz, an Investigator at the Howard Hughes Medical Institute in the Department of Biology at the Massachusetts Institute of Technology. AriSLA cofinanced with support of "5 × 1000" Healthcare Research of the Ministry of Health (grant NOVALS 2012 to N.T., CT., C.G., V.S., and J.E.L.) and the Italian Ministry of Health (grant GR-2011–02347820-IRisALS to N.T. and C.T). The views expressed are those of the authors and not necessarily those of the NHS, the NIHR, or the Department of Health. Funding was provided by the NIH/NINDS (R01NS073873 to J.E.L.), the American ALSA, and Project MinE. Funding was also provided by Instituto de Salud Carlos III (grant PI14/00088) and FUNDELA (Spanish foundation for the development of ALS research). The work leading up to this publication was funded by the European Community's Health Seventh Framework Programme (FP7/2007–2013; grant agreement number 259867). Samples used in this research were, in part, obtained from the U.K. National DNA Bank for Motor Neuron Disease (MND) Research, funded by the MND Association and the Wellcome Trust.

REFERENCES AND NOTES

1. Abhinav K, Stanton B, Johnston C, Hardstaff J, Orrell RW, Howard R, Clarke J, Sakel M, Ampong M-A, Shaw CE, Leigh PN, Al-Chalabi A, Amyotrophic lateral sclerosis in South-East England: A population-based study. The South-East England register for amyotrophic lateral sclerosis (SEALS Registry). Neuroepidemiology 29, 44–48 (2007). [PubMed: 17898523]
2. Smith BN, Newhouse S, Shatunov A, Vance C, Topp S, Johnson L, Miller J, Lee Y, Troakes C, Scott KM, Jones A, Gray I, Wright J, Hortobágyi T, Al-Sarraj S, Rogelj B, Powell J, Lupton M, Lovestone S, Sapp PC, Weber M, Nestor PJ, Schelhaas HJ, ten Asbroek AALM, Silani V, Gellera C, Taroni F, Ticozzi N, Van den Berg L, Veldink J, Van Damme P, Robberecht W, Shaw PJ, Kirby J, Pall H, Morrison KE, Morris A, de Belleroche J, Vianney de Jong JMB, Baas F, Andersen PM, Landers J, Brown RH Jr., Weale ME, Al-Chalabi A, Shaw CE, The *C9ORF72* expansion mutation is a common cause of ALS+/−FTD in Europe and has a single founder. Eur. J. Hum. Genet 21, 102–108 (2013). [PubMed: 22692064]
3. Al-Chalabi A, Jones A, Troakes C, King A, Al-Sarraj S, van den Berg LH, The genetics and neuropathology of amyotrophic lateral sclerosis. Acta Neuropathol. 124, 339–352 (2012). [PubMed: 22903397]
4. White MA, Sreedharan J, Amyotrophic lateral sclerosis: Recent genetic highlights. Curr. Opin. Neurol 29, 557–564 (2016). [PubMed: 27538057]
5. Wu C-H, Fallini C, Ticozzi N, Keagle PJ, Sapp PC, Piotrowska K, Lowe P, Koppers M, McKenna-Yasek D, Baron DM, Kost JE, Gonzalez-Perez P, Fox AD, Adams J, Taroni F, Tiloca C, Leclerc AL, Chafe SC, Mangroo D, Moore MJ, Zitzewitz JA, Xu Z-S, van den Berg LH, Glass JD, Siciliano G, Cirulli ET, Goldstein DB, Salachas F, Meininger V, Rossoll W, Ratti A, Gellera C, Bosco DA, Bassell GJ, Silani V, Drory VE, Brown RH Jr., J. E. Landers, Mutations in the profilin 1 gene cause familial amyotrophic lateral sclerosis. Nature 488, 499–503 (2012). [PubMed: 22801503]
6. Johnson JO, Pioro EP, Boehringer A, Chia R, Feit H, Renton AE, Pliner HA, Abramzon Y, Marangi G, Winborn BJ, Gibbs JR, Nalls MA, Morgan S, Shoai M, Hardy J, Pittman A, Orrell RW, Malaspina A, Sidle KC, Fratta P, Harms MB, Baloh RH, Pestronk A, Weihl CC, Rogaeva E, Zinman L, Drory VE, Borghero G, Mora G, Calvo A, Rothstein JD; ITALSGEN Consortium, Drepper C, Sendtner M, Singleton AB, Taylor JP, Cookson MR, Restagno G, Sabatelli M, Bowser R, Chio A, Traynor BJ, Mutations in the Matrin 3 gene cause familial amyotrophic lateral sclerosis. Nat. Neurosci 17, 664–666 (2014). [PubMed: 24686783]
7. Bannwarth S, Ait-El-Mkadem S, Chaussenot A, Genin EC, Lacas-Gervais S, Fragaki K, Berg-Alonso L, Kageyama Y, Serre V, Moore DG, Verschueren A, Rouzier C, Le Ber I, Augé G, Cochaud C, Lespinasse F, N'Guyen K, de Septenville A, Brice A, Yu-Wai-Man P, Sesaki H, Pouget J, Paquis-Flucklinger V, A mitochondrial origin for frontotemporal dementia and amyotrophic lateral sclerosis through *CHCHD10* involvement. Brain 137, 2329–2345 (2014). [PubMed: 24934289]
8. Johnson JO, Mandrioli J, Benatar M, Abramzon Y, Van Deerlin VM, Trojanowski JQ, Gibbs JR, Brunetti M, Gronka S, Wuu J, Ding J, McCluskey L, Martinez-Lage M, Falcone D, Hernandez DG, Arepalli S, Chong S, Schymick JC, Rothstein J, Landi F, Wang Y-D, Calvo A, Mora G, Sabatelli M,

Monsurrò MR,, Battistini S, Salvi F, Spataro R, Sola P, Borghero G; ITALSGEN Consortium, Galassi G, Scholz SW, Taylor JP, Restagno G, Chiò A, Traynor BJ, Exome sequencing reveals *VCP* mutations as a cause of familial ALS. Neuron 68, 857–864 (2010). [PubMed: 21145000]

9. Smith BN, Ticozzi N, Fallini C, Gkazi AS, Topp S, Kenna KP, Scotter EL, Kost J, Keagle P, Miller JW, Calini D, Vance C, Danielson EW, Troakes C, Tiloca C, Al-Sarraj S, Lewis EA, King A, Colombrita C, Pensato V, Castellotti B, de Belleroche J, Baas F, ten Asbroek ALMA, Sapp PC, McKenna-Yasek D, McLaughlin RL, Polak M, Asress S, Esteban-Pérez J, Muñoz-Blanco JL, Simpson M; SLAGEN Consortium, van Rheenen W, Diekstra FP, Lauria G, Duga S, Corti S, Cereda C, Corrado L, Sorarù G, Morrison KE, Williams KL, Nicholson GA, Blair IP, Dion PA, Leblond CS, Rouleau GA, Hardiman O, Veldink JH, van den Berg LH, Al-Chalabi A, Pall H, Shaw PJ, Turner MR, Talbot K, Taroni F, García-Redondo A, Wu Z, Glass JD, Gellera C, Ratti A, Brown RH Jr., Silani V, Shaw CE, Landers JE, Exome-wide rare variant analysis identifies TUBA4A mutations associated with familial ALS. Neuron 84, 324–331 (2014). [PubMed: 25374358]
10. Cirulli ET, Lasseigne BN, Petrovski S, Sapp PC, Dion PA, Leblond CS, Couthouis J, Lu Y-F, Wang Q, Krueger BJ, Ren Z, Keebler J, Han Y, Levy SE, Boone BE, Wimbish JR, Waite LL, Jones AL, Carulli JP, Day-Williams AG, Staropoli JF, Xin WW, Chesi A, Raphael AR, McKenna-Yasek D, Cady J, Vianney de Jong JMB, Kenna KP, Smith BN, Topp S, Miller J, Gkazi A; FALS Sequencing Consortium, Al-Chalabi A, van den Berg LH, Veldink J, Silani V, Ticozzi N, Shaw CE, Baloh RH, Appel S, Simpson E, Lagier-Tourenne C, Pulst SM, Gibson S, Trojanowski JQ, Elman L, McCluskey L, Grossman M, Shneider NA, Chung WK, Ravits JM, Glass JD, Sims KB, Van Deerlin VM, Maniatis T, Hayes SD, Ordureau A, Swarup S, Landers J, Baas F, Allen AS, Bedlack RS, Harper JW, Gitler AD, Rouleau GA, Brown R, Harms MB, Cooper GM, Harris T, Myers RM, Goldstein DB, Exome sequencing in amyotrophic lateral sclerosis identifies risk genes and pathways. Science 347, 1436–1441 (2015). [PubMed: 25700176]
11. Freischmidt A, Wieland T, Richter B, Ruf W, Schaeffer V, Müller K, Marroquin N, Nordin F, Hübers A, Weydt P, Pinto S, Press R, Millecamps S, Molko N, Bernard E, Desnuelle C, Soriani M-H, Dorst J, Graf E, Nordström U, Feiler MS, Putz S, Boeckers TM, Meyer T, Winkler AS, Winkelman J, de Carvalho M, Thal DR, Otto M, Brännström T, Volk AE, Kursula P, Danzer KM, Lichtner P, Dikic I, Meitinger T, Ludolph AC, Strom TM, Andersen PM, Weishaupt JH, Haploinsufficiency of *TBK1* causes familial ALS and fronto-temporal dementia. Nat. Neurosci 18, 631–636 (2015). [PubMed: 25803835]
12. Kenna KP, van Doormaal PTC, Dekker AM, Ticozzi N, Kenna BJ, Diekstra FP, van Rheenen W, van Eijk KR, Jones AR, Keagle P, Shatunov A, Sproviero W, Smith BN, van Es MA, Topp SD, Kenna A, Miller JW, Fallini C, Tiloca C, McLaughlin RL, Vance C, Troakes C, Colombrita C, Mora G, Calvo A, Verde F, Al-Sarraj S, King A, Calini D, de Belleroche J, Baas F, van der Kooi AJ, de Visser M, ten Asbroek ALMA, Sapp PC, McKenna-Yasek D, Polak M, Asress S, Muñoz-Blanco JL, Strom TM, Meitinger T, Morrison KE; SLAGEN Consortium, G., Williams KL, Leigh PN, Nicholson GA, Blair IP, Leblond CS, Dion PA, Rouleau GA, Pall H, Shaw PJ, Turner MR, Talbot K, Taroni F, Boylan KB, Van Blitterswijk M, Rademakers R, Esteban-Pérez J, Garcia-Redondo A, Van Damme P, Robberecht W, Chio A, Gellera C, Drepper C, Sendtner M, Ratti A, Glass JD, Mora JS, Basak NA, Hardiman O, Ludolph AC, Andersen PM, Weishaupt JH, Brown RH Jr., Al-Chalabi A, Silani V, Shaw CE, van den Berg LH, Veldink JH, Landers JE, *NEK1* variants confer susceptibility to amyotrophic lateral sclerosis. Nat. Genet 48, 1037–1042 (2016). [PubMed: 27455347]
13. Brenner D, Müller K, Wieland T, Weydt P, Böhm S, Lulé D, Hübers A, Neuwirth C, Weber M, Borck G, Wahlqvist M, Danzer KM, Volk AE, Meitinger T, Strom TM, Otto M, Kassubek J, Ludolph AC, Andersen PM, Weishaupt JH, *NEK1* mutations in familial amyotrophic lateral sclerosis. Brain 139, e28 (2016). [PubMed: 26945885]
14. Williams KL, Topp S, Yang S, Smith B, Fifita JA, Warraich ST, Zhang KY, Farrawell N, Vance C, Hu X, Chesi A, Leblond CS, Lee A, Rayner SL, Sundaramoorthy V, Dobson-Stone C, Molloy MP, van Blitterswijk M, Dickson DW, Petersen RC, Graff-Radford NR, Boeve BF, Murray ME, Pottier C, Don E, Winnick C, McCann EP, Hogan A, Daoud H, Levert A, Dion PA, Mitsui J, Ishiura H, Takahashi Y, Goto J, Kost J, Gellera C, Gkazi AS, Miller J, Stockton J, Brooks WS, Boundy K, Polak M, Muñoz-Blanco JL, Esteban-Perez J, Rábano A, Hardiman O, Morrison KE, Ticozzi N, Silani V, de Belleroche J, Glass JD, Kwok JBJ, Guillemin GJ, Chung RS, Tsuji S, Brown RH Jr., García-Redondo A, Rademakers R, Landers JE, Gitler AD, Rouleau GA, Cole NJ, Yerbury JJ,

Atkin JD, Shaw CE, Nicholson GA, Blair IP, CCNF mutations in amyotrophic lateral sclerosis and frontotemporal dementia. Nat. Commun 7, 11253 (2016). [PubMed: 27080313]

15. van Rheenen W, Shatunov A, Dekker AM, McLaughlin RL, Diekstra FP, Pulit SL, van der Spek RA, Võsa U, de Jong S, Robinson MR, Yang J, Fogh I, van Doormaal PTC, Tazelaar GHP, Koppers M, Blokhuis AM, Sproviero W, Jones AR, Kenna KP, van Eijk KR, Harschnitz O, Schellevis RD, Brands WJ, Medic J, Menelaou A, Vajda A, Ticozzi N, Lin K, Rogelj B, Vrabec K, Ravnik-Glavač M, Koritnik B, Zidar J, Leonardis L, Grošelj LD, Millecamps S, Salachas F, Meininger V, de Carvalho M, Pinto S, Mora JS, Rojas-García R, Polak M, Chandran S, Colville S, Swingler R, Morrison KE, Shaw PJ, Hardy J, Orrell RW, Pittman A, Sidle K, Fratta P, Malaspina A, Topp S, Petri S, Abdulla S, Drepper C, Sendtner M, Meyer T, Ophoff RA, Staats KA, Wiedau-Pazos M, Lomen-Hoerth C, Van Deerlin VM, Trojanowski JQ, Elman L, McCluskey L, Basak AN, Tunca C, Hamzeiy H, Parman Y, Meitinger T, Lichtner P, Radivojkov-Blagojevic M, Andres CR, Maurel C, Bensimon G, Landwehrmeyer B, Brice A, Payan CAM, Saker-Delye S, Dürr A, Wood NW, Tittmann L, Lieb W, Franke A, Rietschel M, Cichon S, Nöthen MM, Amouyel P, Tzourio C, Dartigues J-F, Uitterlinden AG, Rivadeneira F, Estrada K, Hofman A, Curtis C, Blauw HM, van der Kooi AJ, de Visser M, Goris A, Weber M, Shaw CE, Smith BN, Pansarasa O, Cereda C, Del Bo R, Comi GP, D'Alfonso S, Bertolin C, Sorarù G, Mazzini L, Pensato V, Gellera C, Tiloca C, Ratti A, Calvo A, Moglia C, Brunetti M, Arcuti S, Capozzo R, Zecca C, Lunetta C, Penco S, Riva N, Padovani A, Filosto M, Muller B, Stuit RJ; PARALS Registry; SLALOM Group; SLAP Registry; FALS Sequencing Consortium; SLAGEN Consortium; NNIPPS Study Group, Blair I, Zhang K, McCann EP, Fifita JA, Nicholson GA, Rowe DB, Pamphlett R, Kiernan MC, Grosskreutz J, Witte OW, Ringer T, Prell T, Stubendorff B, Kurth I, Hübner CA, Leigh PN, Casale F, Chio A, Beghi E, Pupillo E, Tortelli R, Logroscino G, Powell J, Ludolph AC, Weishaupt JH, Robberecht W, Van Damme P, Franke L, Pers TH, Brown RH, Glass JD, Landers JE, Hardiman O, Andersen PM, Corcia P, Vourc'h P, Silani V, Wray NR, Visscher PM, de Bakker PIW, van Es MA, Pasterkamp RJ, Lewis CM, Breen G, Al-Chalabi A, van den Berg LH, Veldink JH, Genome-wide association analyses identify new risk variants and the genetic architecture of amyotrophic lateral sclerosis. Nat. Genet 48, 1043–1048 (2016). [PubMed: 27455348]
16. Gerke V, Moss SE, Annexins: From structure to function. Physiol. Rev 82, 331–371 (2002). [PubMed: 11917092]
17. Rezvanpour A, Shaw GS, Unique S100 target protein interactions. Gen. Physiol. Biophys 28, F39–F46 (2009). [PubMed: 20093725]
18. Wang J, Guo C, Liu S, Qi H, Yin Y, Liang R, Sun M-Z, Greenaway FT, Annexin A11 in disease. Clin. Chim. Acta 431, 164–168 (2014). [PubMed: 24508622]
19. Hofmann S, Franke A, Fischer A, Jacobs G, Nothnagel M, Gaede KI, Schürmann M, Müller-Quernheim J, Krawczak M, Rosenstiel P, Schreiber S, Genome-wide association study identifies *ANXA11* as a new susceptibility locus for sarcoidosis. Nat. Genet 40, 1103–1106 (2008). [PubMed: 19165924]
20. Lek M, Karczewski KJ, Minikel EV, Samocha KE, Banks E, Fennell T, O'Donnell-Luria AH, Ware JS, Hill AJ, Cummings BB, Tukiainen T, Birnbaum DP, Kosmicki JA, Duncan LE, Estrada K, Zhao F, Zou J, Pierce-Hoffman E, Berghout J, Cooper DN, Deflaux N, DePristo M, Do R, Flannick J, Fromer M, Gauthier L, Goldstein J, Gupta N, Howrigan D, Kiezun A, Kurki MI, Moonshine AL, Natarajan P, Orozco L, Peloso GM, Poplin R, Rivas MA, Ruano-Rubio V, Rose SA, Ruderfer DM, Shakir K, Stenson PD, Stevens C, Thomas BP, Tiao G, Tusie-Luna MT, Weisburd B, Won H-H, Yu D, Altshuler DM, Ardissino D, Boehnke M, Danesh J, Donnelly S, Elosua R, Florez JC, Gabriel SB, Getz G, Glatt SJ, Hultman CM, Kathiresan S, Laakso M, McCarroll S, McCarthy MI, McGovern D, McPherson R, Neale BM, Palotie A, Purcell SM, Saleheen D, Scharf JM, Sklar P, Sullivan PF, Tuomilehto J, Tsuang MT, Watkins HC, Wilson JG, Daly MJ, MacArthur DG; Exome Aggregation Consortium, Analysis of protein-coding genetic variation in 60,706 humans. Nature 536, 285–291 (2016). [PubMed: 27535533]
21. Enayat ZE, Orrell RW, Claus A, Ludolph A, Bachus R, Brockmüller J, Ray-Chaudhuri K, Radunovic A, Shaw C, Wilkinson J, Wilkinson J, King A, Swash M, Leigh PN, de Belleroche J, Powell J, Two novel mutations in the gene for copper zinc superoxide dismutase in UK families with amyotrophic lateral sclerosis. Hum. Mol. Genet 4, 1239–1240 (1995). [PubMed: 8528216]
22. Kabashi E, Valdmanis PN, Dion P, Spiegelman D, McConkey BJ, Vande Velde C, Bouchard J-P, Lacomblez L, Pochigaeva K, Salachas F, Pradat P-F, Camu W, Meininger V, Dupre N, Rouleau

GA, *TARDBP* mutations in individuals with sporadic and familial amyotrophic lateral sclerosis. Nat. Genet 40, 572–574 (2008). [PubMed: 18372902]

23. Kwiatkowski TJ Jr., Bosco DA, Leclerc AL, Tamrazian E, Vanderburg CR, Russ C, Davis A, Gilchrist J, Kasarskis EJ, Munsat T, Valdmanis P, Rouleau GA, Hosler BA, Cortelli P, de Jong PJ, Yoshinaga Y, Haines JL, Pericak-Vance MA, Yan J, Ticozzi N, Siddique T, McKenna-Yasek D, Sapp PC, Horvitz HR, Landers JE, Brown RH Jr., Mutations in the *FUS/TLS* gene on chromosome 16 cause familial amyotrophic lateral sclerosis. Science 323, 1205–1208 (2009). [PubMed: 19251627]
24. Puls I, Jonnakuty C, LaMonte BH, Holzbaur ELF, Tokito M, Mann E, Floeter MK, Bidus K, Drayna D, Oh SJ, Brown RH Jr., Ludlow CL, Fischbeck KH, Mutant dynactin in motor neuron disease. Nat. Genet 33, 455–456 (2003). [PubMed: 12627231]
25. Sreedharan J, Blair IP, Tripathi VB, Hu X, Vance C, Rogelj B, Ackerley S, Durnall JC, Williams KL, Buratti E, Baralle F, de Belleroche J, Mitchell JD, Leigh PN, Al-Chalabi A, Miller CC, Nicholson G, Shaw CE, TDP-43 mutations in familial and sporadic amyotrophic lateral sclerosis. Science 319, 1668–1672 (2008). [PubMed: 18309045]
26. Rosen DR, Siddique T, Patterson D, Figlewicz DA, Sapp P, Hentati A, Donaldson D, Goto J, O'Regan JP, Deng HX, Rahmani Z, Krizus A, McKenna-Yasek D, Cayabyab A, Gaston SM, Berger R, Tanzi RE, Halperin JJ, Herzfeldt B, Van den Bergh R, Hung W-Y, Bird T, Deng G, Mulder DW, Smyth C, Laing NG, Soriano E, Pericak-Vance MA, Haines J, Rouleau GA, Gusella JS, Horvitz HR, Brown RH Jr., Mutations in Cu/Zn superoxide dismutase gene are associated with familial amyotrophic lateral sclerosis. Nature 362, 59–62 (1993). [PubMed: 8446170]
27. Deng HX, Hentati A, Tainer JA, Iqbal Z, Cayabyab A, Hung WY, Getzoff ED, Hu P, Herzfeldt B, Roos RP, Warner C, Deng G, Soriano E, Smyth C, Parge HE, Ahmed A, Roses AD, Hallewell RA, Pericak-Vance MA, Siddique T, Amyotrophic lateral sclerosis and structural defects in Cu,Zn superoxide dismutase. Science 261, 1047–1051 (1993). [PubMed: 8351519]
28. Esteban J, Rosen DR, Bowling AC, Sapp P, McKenna-Yasek D, O'Regan JP, Beal MF, Horvitz HR, Brown RH Jr., Identification of two novel mutations and a new polymorphism in the gene for Cu/Zn superoxide dismutase in patients with amyotrophic lateral sclerosis. Hum. Mol. Genet 3, 997–998 (1994). [PubMed: 7951252]
29. Chiò A, Restagno G, Brunetti M, Ossola I, Calvo A, Mora G, Sabatelli M, Monsurrò MR, Battistini S, Mandrioli J, Salvi F, Spataro R, Schymick J, Traynor BJ, La Bella V; ITALSGEN Consortium, Two Italian kindreds with familial amyotrophic lateral sclerosis due to FUS mutation. Neurobiol. Aging 30, 1272–1275 (2009). [PubMed: 19450904]
30. Abecasis GR, Cherny SS, Cookson WO, Cardon LR, Merlin—Rapid analysis of dense genetic maps using sparse gene flow trees. Nat. Genet 30, 97–101 (2002). [PubMed: 11731797]
31. Ralph P, Coop G, The geography of recent genetic ancestry across Europe. PLOS Biol. 11, e1001555 (2013). [PubMed: 23667324]
32. Mizutani A, Watanabe N, Kitao T, Tokumitsu H, Hidaka H, The long amino-terminal tail domain of annexin XI is necessary for its nuclear localization. Arch. Biochem. Biophys 318, 157–165 (1995). [PubMed: 7726557]
33. Leśniak W, Słomnicki ŁP, Filipek A, S100A6—New facts and features. Biochem. Biophys. Res. Commun 390, 1087–1092 (2009). [PubMed: 19891957]
34. Sudo T, Hidaka H, Characterization of the calcyclin (S100A6) binding site of annexin XI-A by site-directed mutagenesis. FEBS Lett. 444, 11–14 (1999). [PubMed: 10037139]
35. Drozdetskiy A, Cole C, Procter J, Barton GJ, JPred4: A protein secondary structure prediction server. Nucleic Acids Res. 43, W389–W394 (2015). [PubMed: 25883141]
36. Lecona E, Turnay J, Olmo N, Guzmán-Aránguez A, Morgan RO, Fernandez M-P, Lizarbe MA, Structural and functional characterization of recombinant mouse annexin A11: Influence of calcium binding. Biochem. J 373, 437–449 (2003). [PubMed: 12689336]
37. Gerke V, Creutz CE, Moss SE, Annexins: Linking Ca^{2+} signalling to membrane dynamics. Nat. Rev. Mol. Cell Biol 6, 449–461 (2005). [PubMed: 15928709]
38. Rosengarth A, Luecke H, A calcium-driven conformational switch of the N-terminal and core domains of annexin A1. J. Mol. Biol 326, 1317–1325 (2003). [PubMed: 12595246]

39. Osako Y, Maemoto Y, Tanaka R, Suzuki H, Shibata H, Maki M, Autolytic activity of human calpain 7 is enhanced by ESCRT-III-related protein IST1 through MIT-MIM interaction. FEBS J. 277, 4412–4426 (2010). [PubMed: 20849418]
40. Hoyaux D, Boom A, Van den Bosch L, Belot N, Martin J-J, Heizmann CW, Kiss R, Pochet R, S100A6 overexpression within astrocytes associated with impaired axons from both ALS mouse model and human patients. J. Neuropathol. Exp. Neurol 61, 736–744 (2002). [PubMed: 12152788]
41. Hoyaux D, Alao J, Fuchs J, Kiss R, Keller B, Heizmann CW, Pochet R, Frermann D, S100A6, a calcium- and zinc-binding protein, is overexpressed in SOD1 mutant mice, a model for amyotrophic lateral sclerosis. Biochim. Biophys. Acta 1498, 264–272 (2000). [PubMed: 11108968]
42. Al-Chalabi A, Andersen PM, Chioza B, Shaw C, Sham PC, Robberecht W, Matthijs G, Camu W, Marklund SL, Forsgren L, Rouleau G, Laing NG, Hurse PV, Siddique T, Leigh PN, Powell JF, Recessive amyotrophic lateral sclerosis families with the D90A *SOD1* mutation share a common founder: Evidence for a linked protective factor. Hum. Mol. Genet 7, 2045–2050 (1998). [PubMed: 9817920]
43. Nishimura AL, Al-Chalabi A, Zatz M, A common founder for amyotrophic lateral sclerosis type 8 (ALS8) in the Brazilian population. Hum. Genet 118, 499–500 (2005). [PubMed: 16187141]
44. Chiò A, Borghero G, Pugliatti M, Ticca A, Calvo A, Moglia C, Mutani R, Brunetti M, Ossola I, Marrosu MG, Murru MR, Floris G, Cannas A, Parish LD, Cossu P, Abramzon Y, Johnson JO, Nalls MA, Arepalli S, Chong S, Hernandez DG, Traynor BJ, Restagno G; Italian Amyotrophic Lateral Sclerosis Genetic (ITALSGEN) Consortium, Large proportion of amyotrophic lateral sclerosis cases in Sardinia due to a single founder mutation of the TARDBP gene. Arch. Neurol 68, 594–598 (2011). [PubMed: 21220647]
45. Tomas A, Futter C, Moss SE, Annexin 11 is required for midbody formation and completion of the terminal phase of cytokinesis. J. Cell Biol 165, 813–822 (2004). [PubMed: 15197175]
46. Shibata H, Kanadome T, Sugiura H, Yokoyama T, Yamamuro M, Moss SE, Maki M, A new role for annexin A11 in the early secretory pathway via stabilizing Sec31A protein at the endoplasmic reticulum exit sites (ERES). J. Biol. Chem 290, 4981–4993 (2015). [PubMed: 25540196]
47. Fukushima T, Zapata JM, Singha NC, Thomas M, Kress CL, Krajewska M, Krajewski S, Ronai Z, Reed JC, S.-i. Matsuzawa, Critical function for SIP, a ubiquitin E3 ligase component of the β-catenin degradation pathway, for thymocyte development and G1 checkpoint. Immunity 24, 29–39 (2006). [PubMed: 16413921]
48. Polymenidou M, Lagier-Tourenne C, Hutt KR, Huelga SC, Moran J, Liang TY, Ling S-C, Sun E, Wancewicz E, Mazur C, Kordasiewicz H, Sedaghat Y, Donohue JP, Shiue L, Bennett CF, Yeo GW, Cleveland DW, Long pre-mRNA depletion and RNA missplicing contribute to neuronal vulnerability from loss of TDP-43. Nat. Neurosci 14, 459–468 (2011). [PubMed: 21358643]
49. Ling JP, Pletnikova O, Troncoso JC, Wong PC, TDP-43 repression of nonconserved cryptic exons is compromised in ALS-FTD. Science 349, 650–655 (2015). [PubMed: 26250685]
50. Botelho HM, Leal SS, Cardoso I, Yanamandra K, Morozova-Roche LA, Fritz G, Gomes CM, S100A6 amyloid fibril formation is calcium-modulated and enhances superoxide dismutase-1 (SOD1) aggregation. J. Biol. Chem 287, 42233–42242 (2012). [PubMed: 23076148]
51. Prell T, Lautenschläger J, Grosskreutz J, Calcium-dependent protein folding in amyotrophic lateral sclerosis. Cell Calcium 54, 132–143 (2013). [PubMed: 23764168]
52. Brooks BR, Miller RG, Swash M, Munsat TL; World Federation of Neurology Research Group on Motor Neuron Diseases, El Escorial revisited: Revised criteria for the diagnosis of amyotrophic lateral sclerosis. Amyotroph. Lateral Scler. Other Motor Neuron Disord 1, 293–299 (2000). [PubMed: 11464847]
53. Wang K, Li M, Hakonarson H, ANNOVAR: Functional annotation of genetic variants from high-throughput sequencing data. Nucleic Acids Res. 38, e164 (2010). [PubMed: 20601685]
54. Purcell S, Neale B, Todd-Brown K, Thomas L, Ferreira MAR, Bender D, Maller J, Sklar P, de Bakker PIW, Daly MJ, Sham PC, PLINK: A tool set for whole-genome association and population-based linkage analyses. Am. J. Hum. Genet 81, 559–575 (2007). [PubMed: 17701901]
55. Yu Y, Triebwasser MP, Wong EKS, Schramm EC, Thomas B, Reynolds R, Mardis ER, Atkinson JP, Daly M, Raychaudhuri S, Kavanagh D, Seddon JM, Whole-exome sequencing identifies rare,

functional *CFH* variants in families with macular degeneration. Hum. Mol. Genet 23, 5283–5293 (2014). [PubMed: 24847005]

56. Down TA, Piipari M, Hubbard TJP, Dalliance: Interactive genome viewing on the web. Bioinformatics 27, 889–890 (2011). [PubMed: 21252075]
57. Tomas A, Moss SE, Calcium- and cell cycle-dependent association of annexin 11 with the nuclear envelope. J. Biol. Chem 278, 20210–20216 (2003). [PubMed: 12601007]
58. Shibata H, Inuzuka T, Yoshida H, Sugiura H, Wada I, Maki M, The ALG-2 binding site in Sec31A influences the retention kinetics of Sec31A at the endoplasmic reticulum exit sites as revealed by live-cell time-lapse imaging. Biosci. Biotechnol. Biochem 74, 1819–1826 (2010). [PubMed: 20834162]
59. Katoh K, Shibata H, Suzuki H, Nara A, Ishidoh K, Kominami E, Yoshimori T, Maki M, The ALG-2-interacting protein Alix associates with CHMP4b, a human homologue of yeast Snf7 that is involved in multivesicular body sorting. J. Biol. Chem 278, 39104–39113 (2003). [PubMed: 12860994]
60. Okumura M, Ichioka F, Kobayashi R, Suzuki H, Yoshida H, Shibata H, Maki M, Penta-EF-hand protein ALG-2 functions as a Ca^{2+}-dependent adaptor that bridges Alix and TSG101. Biochem. Biophys. Res. Commun 386, 237–241 (2009). [PubMed: 19520058]
61. Shibata H, Suzuki H, Yoshida H, Maki M, ALG-2 directly binds Sec31A and localizes at endoplasmic reticulum exit sites in a Ca^{2+}-dependent manner. Biochem. Biophys. Res. Commun 353, 756–763 (2007). [PubMed: 17196169]
62. Fallini C, Bassell GJ, Rossoll W, High-efficiency transfection of cultured primary motor neurons to study protein localization, trafficking, and function. Mol. Neurodegener 5, 17 (2010). [PubMed: 20406490]
63. Smith BN, Vance C, Scotter EL, Troakes C, Wong CH, Topp S, Maekawa S, King A, Mitchell JC, Lund K, Al-Chalabi A, Ticozzi N, Silani V, Sapp P, Brown RH Jr., Landers JE, Al-Sarraj S, Shaw CE, Novel mutations support a role for *Profilin 1* in the pathogenesis of ALS. Neurobiol. Aging 36, 1602.e17–1602.e27 (2015).
64. Chen H-J, Mitchell JC, Novoselov S, Miller J, Nishimura AL, Scotter EL, Vance CA, Cheetham ME, Shaw CE, The heat shock response plays an important role in TDP-43 clearance: Evidence for dysfunction in amyotrophic lateral sclerosis. Brain 139, 1417–1432 (2016). [PubMed: 26936937]
65. Maekawa S, Leigh PN, King A, Jones E, Steele JC, Bodi I, Shaw CE, Hortobagyi T, Al-Sarraj S, TDP-43 is consistently co-localized with ubiquitinated inclusions in sporadic and Guam amyotrophic lateral sclerosis but not in familial amyotrophic lateral sclerosis with and without SOD1 mutations. Neuropathology 29, 672–683 (2009). [PubMed: 19496940]

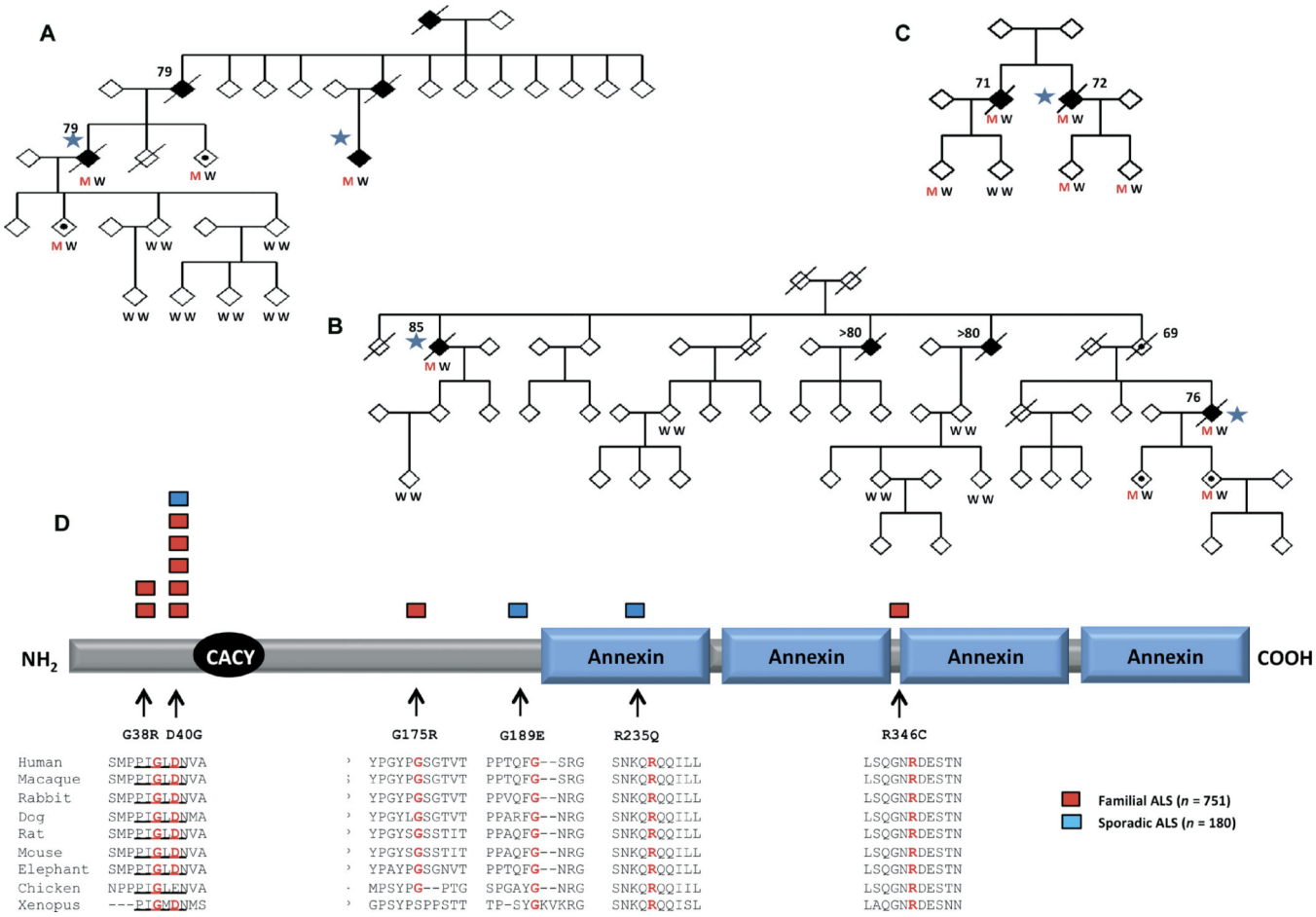

Fig. 1. Annexin A11 mutations identified in ALS patients after stringent filtering of exome sequencing data.

(**A** and **B**) Pedigrees of U.K. Family 1 and 2, respectively, carrying the p.D40G mutation. Family members for whom DNA was available for segregation analysis are labeled with M/W for a heterozygous mutation (A > G allele) or W/W for a homozygous reference allele. The gender has been anonymized for each individual. Affected individuals with ALS are denoted by a solid black diamond, unaffected individuals by white diamonds, and unaffected carriers with a black dot. Affected family members who underwent exome sequencing as part of this study are marked with abluestar. (**C**) The p.G175R mutation segregates in both an index case and affected sibling. (A to C) The age at death, where data are available, is listed above each p.D40G carrier (affected and unaffected). (**D**) Schematic representation of the annexin A11 protein highlighting the clustering of mutations in the N terminus (first 196 residues). Mutation positions in the N terminus are fully conserved in mammals and conserved in birds, amphibians, and reptiles if the mutations are in annexin domains. Mutations in FALS are indicated by red boxes and those in SALS by blue boxes. The p.D40G mutation found in two index FALS cases and an affected sibling from each U.K. family, an Italian index case, and a U.K. SALS case ($n = 6$) clusters with the p.G38R mutation in the N terminus of the annexin A11 molecule. The binding site of calcyclin (CACY) is located in the N terminus (residues 50 to 62).

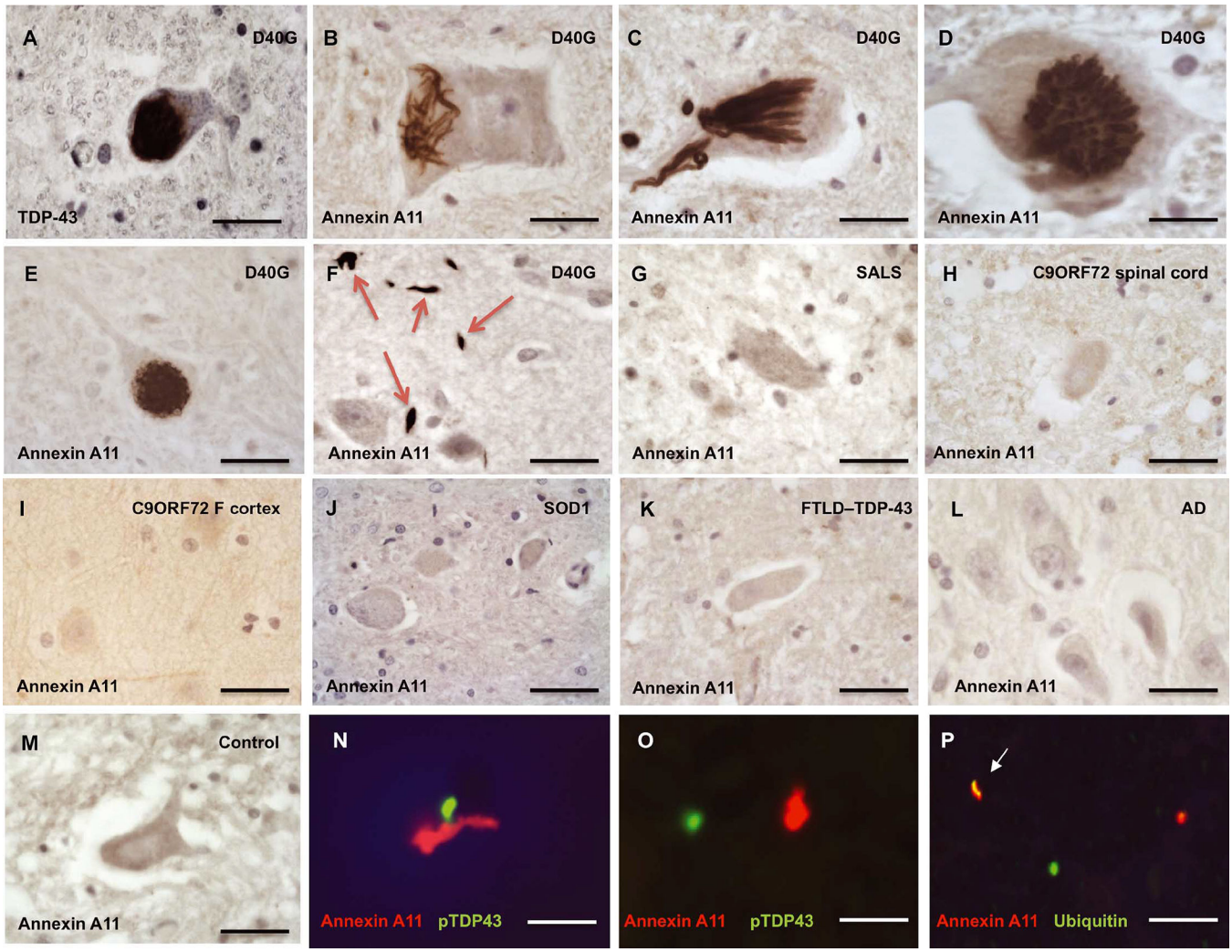

Fig. 2. Annexin A11 immunohistochemical analysis in postmortem spinal cord tissue from a SALS case with the p.D40G mutation.

(**A**) Phospho-TDP-43-positive cytoplasmic inclusion from the anterior horn of the spinal cord. (**B** to **E**) Annexin A11-positive inclusions in motor neurons of the spinal cord include skein-like structures (B) and filamentous and tubular-shaped structures (C and D). Occasional basket-like inclusions were seen in the spinal cord (E). (**F**) Abundant annexin A11-positive torpedo-like neuritic structures were present in the neuropil of the motor cortex (red arrows). Representative spinal cord staining for annexin A11 inclusions in a SALS case (n =15) who is negative for *ANXA11* mutations (**G**) and two *C9ORF72* expansion-positive ALS cases (spinal cord and frontal cortex) (**H** and **I**). (**J**) Staining for annexin A11 inclusions was also negative in an ALS case harboring a p.D101G mutation in *SOD1* (spinal cord). Similarly, frontotemporal lobar degeneration (FTLD)-TDP-43 cases (spinal cord; n = 3) (**K**) and Alzheimer's disease (AD) cases (n = 3) (**L**) and control individuals (n = 13) (**M**) were also negative for staining for annexin A11 inclusions. (**N** and **O**) Double labeling of spinal cord tissue in the p.D40G SALS case for phospho-TDP-43 (green) and annexin A11 aggregates (red). (**P**) Costaining for ubiquitinated aggregates (red, annexin A11; green, ubiquitin) showed occasional colocalization (white arrow). Scale bars, 30 μm (A, E, G, and

H), 20 μm (B and C), 15 μm (D), 50 μm (F, I, J, K, and L), 25 μm (M and N), and 50 μm (O and P).

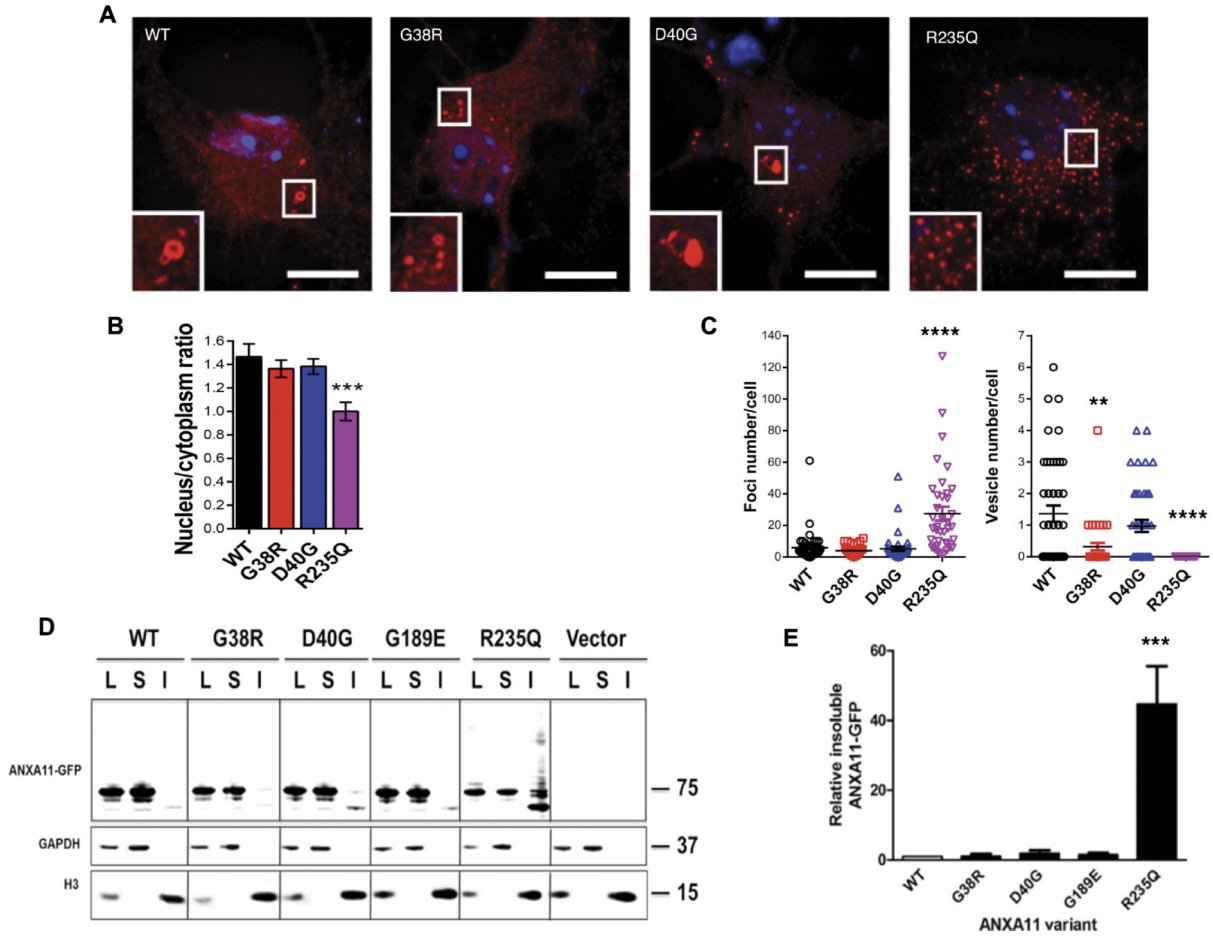

Fig. 3. Transfection of WT and mutant annexin A11 into mouse primary motor neurons and HEK cells.

(**A**) HA tagged annexin A11^{WT}and mutant annexin A11$^{G38R/D40G/R235Q}$ constructs were transfected into mouse primary motor neurons. Transfected cells displayed (A) cytoplasmic vesicle-like structures for annexin A11$^{WT/G38R/D40G}$ and (**B**) increased localization of smaller foci in the cytoplasm of annexin $_{A11}$^{R235Q} transfected neurons [***P = 0.0004, one-way analysis of variance (ANOVA) and Dunnett's post hoc test; bars represent mean and SEM]. Vesicles were defined as structures with a diameter between 0.5 and 1.9 μm (mean, 1 μm) and foci as structures with a diameter between 0.16 and 0.5 μm (mean, 0.3 μm). (**C**) A significant proportion of foci were associated with annexin A11^{R235Q} (****P < 0.0001, one-way ANOVA and Dunnett's post hoc test); a smaller proportion of vesicles were associated with annexin A11^{G38R} and were absent with annexin A11^{R235Q} (**P = 0.0051 and ****P < 0.0001, respectively, one-way ANOVA and Dunnett's post hoc test). (**D**) Transfection of HEK cells with GFP tagged annexin A11$^{WT/G38R/D40G/G189E/R235Q}$ constructs followed by a solubility assay [showing lysate (L), soluble (S), and insoluble (I) fractions] revealed that annexin A11^{R235Q} formed detergent-resistant insoluble aggregates. (**E**) The amount of the annexin A11^{R235Q} insoluble fraction is statistically significant when compared with that for the WT protein (***P = 0.007, one-way ANOVA with Dunnett's post hoc test).

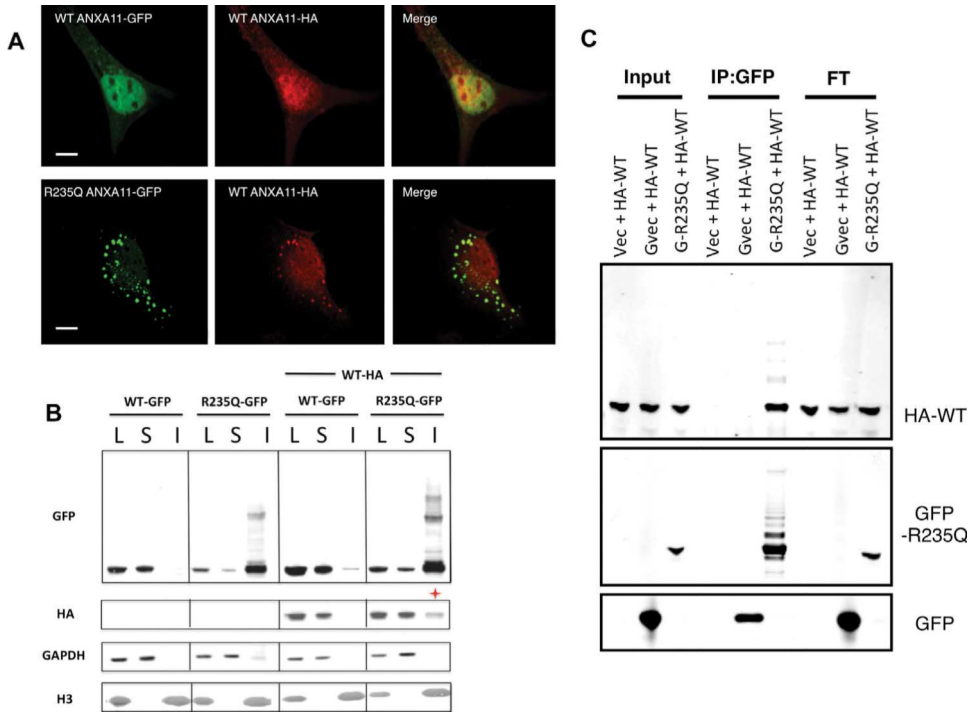

Fig. 4. Annexin A11 with the p.R235Q mutation sequesters WT annexin A11.

(**A**)CoexpressionofANXA11^{WT} tagged with HA and ANXA11^{R235Q} tagged with GFP in SH-SY5Y cells demonstrated colocalization by immunocytohistochemistry, suggesting that the mutant protein sequestered the WT protein. Scale bars, 10 μm. (**B**) To confirm this observation, we conducted solubility assays, generating lysate, soluble, and insoluble fractions, followed by Western blot. Expression of GFP-tagged ANXA11^{WT} and GFP-tagged ANXA11^{R235Q} in HEK cells replicated that seen in Fig. 3D, with aggregates seen only in the insoluble fraction (labeled as I) of ANXA11^{R235Q}. Coexpression of GFP-tagged ANXA11^{WT} or ANXA11^{R235Q} with an equal amount of HA-tagged ANXA11^{WT} in HEK cells resulted in accumulation of HA-tagged ANXA11^{WT} in the insoluble fraction only when coexpressed with GFP-tagged ANXA11^{R235Q} (indicated by a red cross) ($n = 3$). (**C**) A further IP assay also confirmed sequestering of ANXA11^{WT} by ANXA11^{R235Q}. Cotransfection of HEK cells with GFP-tagged ANXA11^{R235Q} and HA-tagged ANXA11^{WT} followed by IP with rabbit anti-GFP antibody, and probing with mouse anti-HA antibody demonstrated direct sequestering of ANXA11^{WT} in the IP fraction. This included higher insoluble molecular weight species compared to control empty plasmid vector and empty plasmid vector plus GFP (top). Verification of the IP was shown by staining with mouse-GFP (input total protein lysate and IP;middle)and positive staining of HA-tagged ANXA11^{WT} [input and nonbound bead flow-through (FT);top].

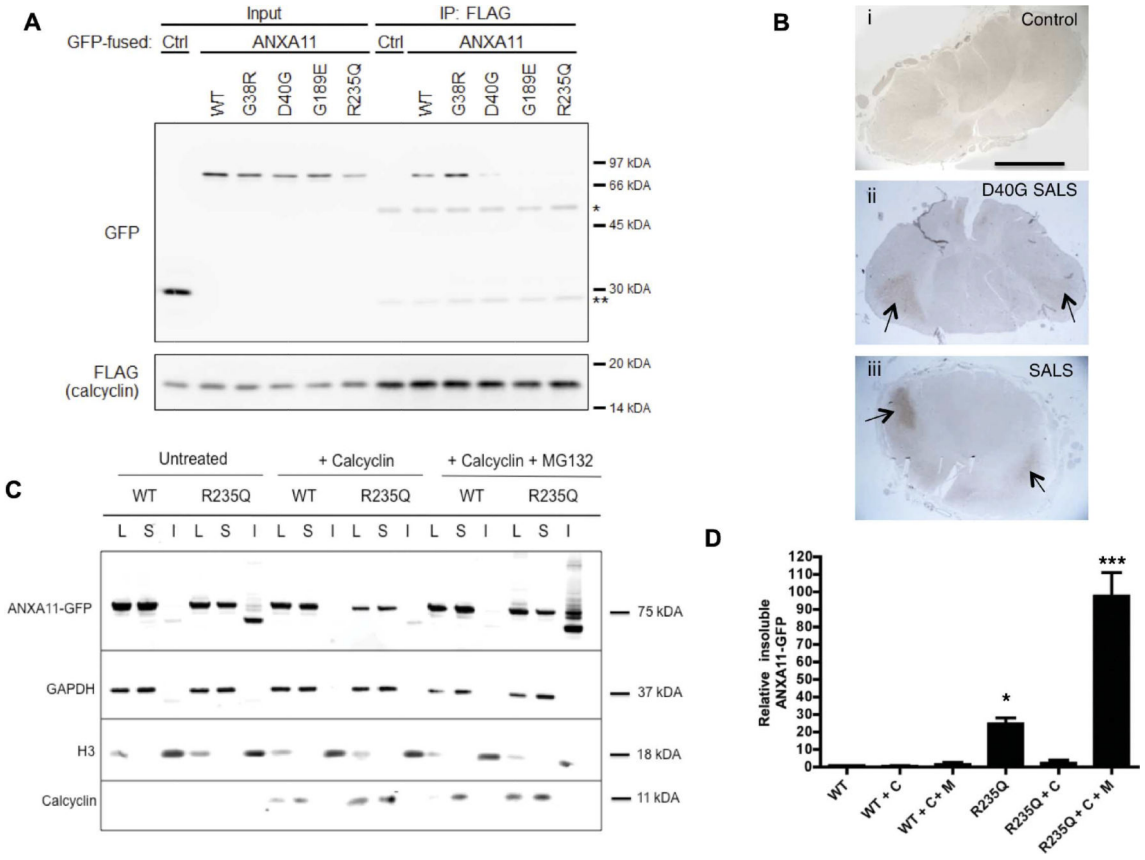

Fig. 5. Annexin A11 mutations disrupt binding to calcyclin.

(**A**) Western blot demonstrating lack of binding of FLAG-tagged calcyclin to GFP-tagged mutant annexin A11 ($ANXA11^{D40G}$, $ANXA11^{G189E}$, and $ANXA11^{R235Q}$) compared to $ANXA11^{WT}$ after IP ($n = 3$).Top: GFP intensities of input and immunoprecipitated fractions, with immunoglobulin G (IgG) heavy [50kDA (*)]and light [25 kDa (**)] chains indicated. Bottom: Input and IP of FLAG-tagged calcyclin alone. Ctrl, control. (**B**) Cross section of postmortem spinal cord tissue showing calcyclin expression in (i) controls and (ii) a SALS case with the p.D40G mutation. High calcyclin expression can be seen in the lateral corticospinal tracts (black arrows). (iii) SALS case with no known ALS causing mutation but displaying strong expression of calcyclin in the lateral corticospinal tracts in postmortem spinal cord (black arrows). Scale bars, 40 μm (i), 30 μm (ii), and 25 μm (iii). (**C**) To determine the effect of calcyclin overexpression on aggregation, we conducted an NP-40 solubility assay by coexpressing 500 ng of GFP-tagged $ANXA11^{WT}$ or $ANXA11^{R235Q}$ and 500 ng of FLAG-tagged calcyclin in HEK cells. Clearance of insoluble p.R235Q mutant annexin A11 aggregates by calcyclin was observed. Addition of the proteasomal inhibitor MG132 restored the aggregation event by blocking degradation of the aggregated proteins by the ubiquitin proteosomal pathway. An equivalent amount of empty GFP vector (500 ng) was added to HEK cells expressing WT or p.R235Q mutant annexin A11 as a loading control. (**D**) Quantification of the proportion of insoluble fractions from (C) relative to untreated $ANXA11^{GFP}$ (WT) including calcyclin overexpression (+C) and calcyclin overexpression plus MG132 treatment (+C +M). Bands were quantified with ImageJ, and

intensity was calculated with respect to untreated GFP-tagged $ANXA11^{WT}$. A one-way ANOVA test demonstrated significance for increased aggregation due to the p.R235Q mutation and rescue of aggregation in p.R235Q mutant cells by calcyclin overexpression and MG132 treatment (R235Q + C + M). $*P < 0.05$ and $***P < 0.001$, respectively, one-way ANOVA and Dunnett's post hoc test ($n = 3$).